Research Square

Preprints are preliminary reports that have not undergone peer review.
They should not be considered conclusive, used to inform clinical practice,
or referenced by the media as validated information.

A history of type 2 diabetes results in immune dysregulation and failure to contain a fatal fungal infection

Ana Traven

ana.traven@monash.edu

Monash University https://orcid.org/0000-0001-6252-3104

Helen Stölting

Monash University https://orcid.org/0000-0002-7830-2776

Antara Ghoshal

Monash University https://orcid.org/0009-0003-5909-3774

Harshini Weerasinghe

Monash University

Yuqin Wu

Monash University https://orcid.org/0000-0002-1762-1896

Patricia Rusu

Monash University https://orcid.org/0000-0001-7210-1976

Dylan Multari

Monash University https://orcid.org/0000-0001-6932-9881

Katherine Jeppe

Monash University https://orcid.org/0000-0003-2284-5090

Christopher Barlow

Monash University https://orcid.org/0000-0001-9309-2829

Ralf Schittenhelm

Monash University https://orcid.org/0000-0001-8738-1878

Kim O'Sullivan

Monash University https://orcid.org/0000-0002-3098-7948

Andre Mu

Monash University

Adam Rose

Monash University https://orcid.org/0000-0001-9132-8244

Article

Keywords: Fungal infection, Candida albicans, glucose metabolism, immune dysfunction, type 2 diabetes, obesity, interferon, NK cells

Posted Date: November 6th, 2026

DOI: https://doi.org/10.21203/rs.3.rs-11302422/v1

License: This work is licensed under a Creative Commons Attribution 4.0 International License. Read Full License

Additional Declarations: Yes there is potential Competing Interest. P.M.R. & A.J.R. have received funding from Boehringer-Ingelheim, a pharmaceutical company, for an unrelated project. The other authors declare no competing interests.

Abstract

Glucose metabolism enables antimicrobial defences, but it also contributes to pathogen proliferation and immune evasion. A key disease of glucose metabolism, type 2 diabetes (T2D), leads to worse outcomes of *Candida albicans* infections with poorly understood mechanisms. Here we used genetic and dietary animal models of T2D and show that, following bloodstream *C. albicans* infection, T2D animals develop strongly exacerbated disease across several T2D aetiologies. Obesity alone (without overt hyperglycaemia) is sufficient to worsen *C. albicans* disease, but it does not fully recapitulate the severity in T2D hosts that are both obese and overtly hyperglycaemic. Mechanistic analyses showed that a convergence of pathogen and host factors leads to poor outcomes in T2D. *C. albicans* exploits poor host glycaemic control through activation of a transcriptional program for glucose utilisation to drive pathogen proliferation. This, combined with dysregulated immunity characterised by increased pro-inflammatory responses and reduced interferon and NK cell signatures, leads to host failure in restricting fungal growth. We further show that life-long metabolic dysregulation, rather than blood glucose levels at infection, drives poor infection outcomes. Our study illuminates host and pathogen mechanisms leading to worse fungal infection in T2D, provides a rich multi-omics resource for understanding fungal infection in metabolic diseases, and suggests that long-term control of metabolic dysregulation, rather than acute lowering of glucose, is essential for improving survival.

SUMMARY

Glucose metabolism enables antimicrobial defences, but it also contributes to pathogen proliferation and immune evasion. A key disease of glucose metabolism, type 2 diabetes (T2D), leads to worse outcomes of infections with poorly understood mechanisms. Here we used genetic and dietary animal models of T2D and show that, following bloodstream infection, T2D animals develop strongly exacerbated disease across several T2D aetiologies. Obesity alone (without overt hyperglycaemia) is sufficient to worsen disease, but it does not fully recapitulate the severity in T2D hosts that are both obese and overtly hyperglycaemic. Mechanistic analyses showed that a convergence of pathogen and host factors leads to poor outcomes in T2D. exploits poor host glycaemic control through activation of a transcriptional program for glucose utilisation to drive pathogen proliferation. This, combined with dysregulated immunity characterised by increased pro-inflammatory responses and reduced interferon and NK cell signatures, leads to host failure in restricting fungal growth. We further show that life-long metabolic dysregulation, rather than blood glucose levels at infection, drives poor infection outcomes. Our study illuminates host and pathogen mechanisms leading to worse fungal infection in T2D, provides a rich multi-omics resource for understanding fungal infection in metabolic diseases, and suggests that long-term control of metabolic dysregulation, rather than acute lowering of glucose, is essential for improving survival.

INTRODUCTION

Metabolic regulation controls antimicrobial immune responses, as well as the physiological and organ adaptations that are required for surviving infections. Fine-tuning of metabolic processes is also important for pathogens to fuel microbial growth and immune evasion[1–4]. Metabolic adaptation is a common feature of infections caused by all pathogen classes, including fungal infections that represent an increasing healthcare threat[1,3,4]. Amongst them, *Candida albicans* is a common human pathogen causing bloodstream infections in hospitalised patients that can progress to fungal sepsis with high mortality[5].

Glucose metabolism is particularly central to the infection process. The availability of glucose and a functioning and adequately regulated fungal glycolytic pathway drive *C. albicans* virulence by promoting fungal proliferation, competition for glucose with immune cells, and the growth of invasive fungal hyphae that lyse macrophages and penetrate host tissues[6–8]. Glucose is also critical for the host by supporting immune effector functions, including the ability of neutrophils, macrophages and monocytes to kill *C. albicans*, produce antifungal cytokines, survive pathogen challenge and entrap *C. albicans* to prevent dissemination[7,9–13]. Perturbing systemic glucose homeostasis by 2-deoxyglucose or metformin worsens survival during bloodstream *C. albicans* infection in mice, underscoring the critical role of glucose in host defences[7,11,13]. The importance of host glucose homeostasis is further underscored by the fact that diabetes commonly predisposes sufferers to mucosal *Candida* infections[14,15]. Diabetes is also found as a comorbidity for patients with bloodstream *Candida* infections (i.e. candidaemia) and was the most common comorbidity in a recent study of candidaemia from the Center for Disease Control and Prevention (CDC)[14,16,17]. This is concerning given that diabetes cases have quadrupled over the last 35 years, now affecting > 10% of the adult population globally and thereby creating a large number of infection-susceptible hosts[18,19].

Most diabetes cases (> 95%) are classified as type 2 diabetes (T2D)[20], which commonly occurs in adulthood, involves insulin resistance and consequent hyperglycaemia and metabolic dysregulation, and is triggered by a combination of environmental, genetic and lifestyle factors. Diabetes and obesity can be successfully treated with therapeutics such as SGLT2 inhibitors and GLP-1 receptor agonists[21]. Nevertheless, the problem persists because most cases (> 80%) occur in developing countries with limited access to these medicines[18]. Indeed, 2022 data from the WHO show that almost 60% of diabetes patients older than 30 years of age remained untreated, meaning that their diabetes was poorly controlled[22].

Despite the increasing risks from the confluence of rising metabolic and infectious diseases, the mechanisms underlying increased susceptibility of T2D hosts to life-threatening infection remain incompletely understood and are likely to be context dependent. For *C. albicans*, the few published studies implicate suboptimal antifungal immunity, such as reduced fungal uptake and killing by phagocytes, but mechanistic insights remain scarce[23–29] and preprints[30,31]. Moreover, although > 95% of diabetes cases are classified as T2D, almost invariably the *C. albicans* studies used animal models of the less common type 1 diabetes (T1D), an early-onset autoimmune disease caused by the loss of insulin-

producing pancreatic β-cells and mimicked in mice by administration of alloxan or streptozotocin to destroy β-cells. To our knowledge, only one study, published 30 years ago, used a T2D model, the obese Zucker rat, showing increased susceptibility to systemic *C. albicans* infection and reduced antifungal killing by neutrophils and macrophages[25]. However, while obese and hyperinsulinaemic, the Zucker rats displayed only moderate hyperglycaemia below T2D levels (~ 12 mM compared to ~ 9.4 mM in controls), meaning that a major feature of T2D was not recapitulated in this model.

To bridge this gap, we examined the consequences and mechanisms of systemic *C. albicans* infection in genetic and diet-induced mouse models of obesity and T2D. Our study illuminates host and pathogen mechanisms that cause poor fungal infection outcomes in obese and T2D hosts, and shows that chronic uncontrolled diabetes and metabolic disease, rather than blood glucose levels at infection, are responsible for poor disease outcomes.

RESULTS

Type 2 diabetes exacerbates disease severity in systemic C. albicans infection

To develop a *C. albicans* infection model for type 2 diabetes (T2D), we used db/db mice, which have a spontaneous loss-of-function mutation in *Lepr* and manifest obesity (median body weight of 46 g on average relative to 22 g in controls) and hyperglycaemia (median blood glucose ~ 28 mM relative to ~ 9 mM in controls) (Fig. 1A). T2D (db/db) and control (db/+ and +/+) mice were infected intravenously with a fixed dose of 1×10^5 CFU of *C. albicans* and monitored for weight loss and clinical signs of illness. Although T2D (db/db) mice are much heavier than the controls and therefore received a lower dose of *C. albicans* per gram of body weight, they displayed worse disease progression, reaching humane endpoints significantly faster than controls (Fig. 1B). Weight loss was the primary disease symptom and reason for euthanasia in control animals; in contrast, T2D animals lost more body weight and displayed significantly more severe clinical scores, including reduced activity, stiff movements and cataracts in one or both eyes (Figs. 1C-D and **S1**A-B). This stark difference was also reflected in kidneys–the main anatomical site of *C. albicans* proliferation–whereby T2D mice displayed worse macroscopic kidney damage than controls (Fig. 1E). Kidney fungal burden was quantified using the fungal housekeeping genes *RDN25* and *18S* relative to the host housekeeping gene *Tbp* (Figs. 1F-G and **S1**C-D). We validated that fungal *RDN25 and 18S* levels strongly correlate with colony-forming units (CFUs) in kidneys (**Figure S1**E). Compared to controls, T2D mice had significantly higher kidney fungal burden, which was independent of time post-infection (Figs. 1F-G and **S1**C-D). In addition, T2D mice displayed a greater reduction in blood glucose levels post-infection, alongside more pronounced anorexia (reduced food intake) (Figs. 1H-I and **S1**F-G).

To address whether exacerbated disease in T2D resulted from an early inability to contain the infection, we infected T2D and control mice with the same fixed dose of *C. albicans* and collected tissues at 24 hours post-infection. T2D animals had higher fungal burden at 24 hours (Fig. 1J), along with more inflammatory foci and fungal hyphae in histology sections (Figs. 1K-N and **S1**H). Infection further

resulted in increased weight loss and a larger decrease in blood glucose levels in T2D compared to control mice (Figs. 1O-P and **S1**I-J). Serum markers of disease severity, aspartate aminotransferase (AST), alanine aminotransferase (ALT) and creatinine, were elevated in T2D mice with or without infection (**Figure S1**K-M). The stress hormone GDF15, which correlates with sepsis severity[32–34], was significantly higher in infected T2D mice relative to infected control mice (Fig. 1Q). Overall, these data show that T2D mice display aggravated disease severity, with an inability to control systemic *C. albicans* infection that manifests early, as well as worsened long-term survival.

High-fat diet-induced obesity worsens Candida disease but only partially recapitulates the T2D phenotype

As is common in humans affected by T2D, db/db mice are both hyperglycaemic and obese. Therefore, we next asked which aspect of the metabolic disorder–obesity, hyperglycaemia or both–is responsible for increased *Candida* disease severity. To uncouple overt hyperglycaemia from obesity, we induced obesity in male wildtype C57BL/6J mice by feeding a high-fat diet (HFD) for 13 or 16 weeks, until the mice reached a body weight of at least 42 g (Fig. 2A). Showing that obesity is uncoupled from overt hyperglycaemia in these animals, blood glucose was only mildly elevated, from ~ 10 mM to ~ 11 mM, and this increase did not reach statistical significance (Fig. 2B). Following infection with *C. albicans*, obese mice had higher kidney fungal burden and serum GDF15 than lean controls (Fig. 2C-D), with a trend towards more inflammatory foci in kidney histology sections (Fig. 2E). However, there was no difference between obese and lean animals in weight loss, infection-induced reduction in blood glucose or infection-induced anorexia (Figs. 2F-G and **S2**A-B). These data show that obesity worsens *C. albicans* disease, but it only partially recapitulates the exacerbated disease severity observed in db/db mice that are both obese and overtly hyperglycaemic.

C. albicans exploits poor glycaemic control in T2D hosts to activate transcriptional programs for glucose utilisation and drive its own growth

We next asked whether diabetes may alter the kidney infection microenvironment in a way that benefits *C. albicans*. To this end, we infected male T2D (db/db) and control mice with 1×10^5 CFU *C. albicans* and collected kidney interstitial fluid for untargeted polar metabolomic analysis (Figs. 3A and **S3**A). Fungal burden was significantly higher in T2D compared to control animals, demonstrating that infection worked as expected (**Figure S3**B-D). Multi-dimensional scaling revealed clear differences in metabolomic profiles between experimental groups (Fig. 3A). At baseline (without infection), glucose, the preferred carbon source for *C. albicans*, was more abundant in T2D kidney interstitia, alongside other sugars such as raffinose and sucrose (Fig. 3B). Amino acids, which can be utilised as carbon and/or nitrogen sources by *C. albicans*, were more abundant in controls (Fig. 3B). Infection had little effect on metabolite levels in control mice (Fig. 3C), but resulted in perturbed metabolite abundance in T2D kidneys, including decreased glucose levels (Fig. 3D-E). This led us to hypothesise that *C. albicans* may exploit the high availability of glucose to fuel its growth in T2D kidneys. Indeed, gene expression of key *C. albicans* glycolytic enzymes (adjusted for fungal burden) was elevated in T2D compared to control kidneys

(Figs. 3F-J and **S3**E). Relative expression of fungal *ECE1*, which encodes the hyphae-associated virulence factor candidalysin[35], was lower in *Candida* from T2D kidneys (Fig. 3K). This result indicates that increased fungal glycolytic gene expression was unlikely to be caused by a global increase in transcription due to more rapid fungal growth in T2D tissue. Furthermore, while increased glucose availability fuels *C. albicans* growth, it does not impact virulence trait expression.

In *C. albicans*, glycolytic gene expression is controlled by two functionally overlapping transcription factors, Tye7 and Gal4[6] (Fig. 3L). While the *tye7*Δ/Δ*gal4*Δ/Δ double mutant maintains normal growth under oxidative conditions where ATP is generated through oxidative phosphorylation, its growth is stunted when energy production is reliant on fermentative breakdown of glucose due to a failure to induce high expression of glucose transporters and glycolytic enzymes[6]. As such, the *tye7*Δ/Δ*gal4*Δ/Δ mutant displays reduced virulence in the mouse systemic model as well as a reduced ability to compete for glucose with immune cells[6,7]. Despite its attenuated virulence, the *tye7*Δ/Δ*gal4*Δ/Δ mutant caused weight loss and anorexia in infected T2D and control animals (**Figure S3**F-G). As with wildtype infection, T2D mice had higher fungal burden than control animals when infected with the *tye7*Δ/Δ*gal4*Δ/Δ mutant (Fig. 3M). Glucose levels in kidneys of T2D mice infected with either the control strain or *tye7*Δ/Δ*gal4*Δ/Δ were lower than in PBS-treated animals (Fig. 3N), indicating perturbed glucose homeostasis and local glucose consumption by pathogen and/or host cells. However, the differences between *tye7*Δ/Δ*gal4*Δ/Δ-infected T2D and control mice were reduced compared to infection with the control *C. albicans* strain (*tye7*Δ/Δ*gal4*Δ/Δ + *TYE7* + *GAL4*) (Fig. 3M and 3O-P). Kidneys of T2D mice displayed a 15.9-fold increase in fungal CFUs for the control *C. albicans* strain and a smaller, 9.6-fold increase for the *tye7*Δ/Δ*gal4*Δ/Δ mutant (Fig. 3M). Consistently, histology showed a ~ 3-fold increase in inflammatory foci in T2D kidneys for the control *C. albicans* strain and no increase for *tye7*Δ/Δ*gal4*Δ/Δ (Fig. 3O). Similarly, there was a 16.1-fold increase in total fungal area per tissue area for the control *C. albicans* strain but only 3.5-fold for *tye7*Δ/Δ*gal4*Δ/Δ (Fig. 3P). Collectively, these data suggest that *C. albicans* leverages Tye7/Gal4-dependent regulation to increase glycolysis, thereby driving its growth in the glucose-rich environment of T2D kidneys. Nevertheless, the *tye7*Δ/Δ*gal4*Δ/Δ mutant still caused worse disease in T2D compared to control animals, suggesting that augmenting pathogen growth in the T2D environment does not fully explain disease exacerbation.

Chronic metabolic disease, not glucose levels per se, increases susceptibility to infection

High blood glucose may not only benefit pathogen growth, but could also affect host disease resistance and tolerance. To determine if blood glucose levels at the time of infection dictate disease outcome, we formulated a diet containing 0.03% of the SGLT2 inhibitor empagliflozin (EMPA; **Figure S4**A), which blocks reabsorption of glucose in the kidneys and is commonly used in the treatment of T2D to lower blood glucose[21]. T2D mice were fed the EMPA-containing or control diet for 7 days prior to infection with *C. albicans* (Fig. 4A). EMPA caused a significant reduction in blood glucose levels (Fig. 4A), although glucose remained over 15 mM in two-thirds of animals and was thus not completely normalised to non-

T2D levels. EMPA also caused a minor and transient decrease in body weight (**Figure S4**B). Despite lower blood glucose levels at the time of infection, EMPA mice showed the same fungal burden, serum GDF15 levels, weight loss and infection-induced reduction in blood glucose as mice fed the control diet (Figs. 4B-C and **S4**C-D). Thus, acute lowering of blood glucose levels in T2D animals is not sufficient to improve infection outcomes, suggesting long-lasting detrimental effects of chronic hyperglycaemia and the associated metabolic dysfunction.

To investigate whether any hyperglycaemic blood glucose levels above the threshold of 15 mM, irrespective of actual values, would render animals more susceptible to fungal infection, we made use of the New Zealand Obese (NZO) mouse model of polygenic obesity and diabetes. All NZO mice develop obesity when maintained on a standard 4%-fat chow diet. In addition, a subset of male NZO mice will develop type 2 diabetes in adulthood, and diabetes onset can be accelerated by feeding animals a purified HFD in place of standard chow[36]. We exploited this characteristic to compare infection outcomes between hyperglycaemic and normoglycaemic obese animals of the same genetic background. Male NZO mice were placed on a HFD and blood glucose levels were repeatedly measured until hyperglycaemia was observed in ~ 50% of animals (Fig. 4D). To account for variability in blood glucose over time, levels were measured again immediately prior to infection with *C. albicans* (Fig. 4D). There were no differences in fungal burden or serum GDF15 levels when stratifying animals by whether they were normoglycaemic or hyperglycaemic (> 15 mM) at infection (Fig. 4E-F), nor in starting weight or weight loss (**Figure S4**E-F). These data once more indicate that blood glucose levels at the time of *C. albicans* infection are not a major driver of disease outcome. Two animals in the cohort had consistently very high blood glucose levels (> 24 mM in the four weeks leading up to infection), and in these animals we observed significantly higher fungal burden and GDF15 serum levels following infection (**Figure S4**G-H). While the animal number is small, these results are consistent with chronic hyperglycaemia and metabolic dysfunction, rather than high blood glucose *per se*, causing worse outcomes of fungal infection.

Type 2 diabetic mice mount antifungal immune responses comparable with those in control animals

Elevated glucose provided an advantage to *C. albicans* for proliferation in T2D kidneys, but this advantage did not fully explain disease exacerbation (Fig. 3). To understand if the T2D environment perturbs host responses, we developed a multi-omics approach to define host transcriptional and proteomic changes in local infection environments in kidneys from T2D mice (Fig. 5A). These experiments were performed on kidneys contralateral to those from male T2D (db/db) and control mice used for interstitial fluid collection for metabolomics in **Fig. 3**. To visualise the data in an interactive manner, we constructed the publicly available, user-friendly **CanDi** (**Can**dida in **Di**abetes) Shiny app, which can be accessed at https://github.com/hstoelting/CanDi.

There was clear separation of the four groups (control and T2D animals, either mock (PBS)- or *C. albicans*-infected) in both the proteomics and transcriptomics analyses (Fig. 5A) and a large degree of congruency between analytes detected by either approach. Infection resulted in the upregulation of 178 proteins and 1154 genes in control animals, of which 151 proteins (84%) and 1027 genes (89%) were also upregulated with infection in T2D mice (Figs. 5B-C and **S5**A-B). Transcripts for several hormones that link metabolism, energy and inflammation were elevated in infected T2D mice relative to controls, including GDF15, IL-6, FGF21 and LCN2 (LCN2 also being detected at the protein level and elevated in infected T2D vs infected control animals) (https://github.com/hstoelting/CanDi). This is consistent with exacerbated inflammation and metabolic dysfunction in infected T2D animals. Gene-set enrichment analysis of infection responses in protein or gene expression identified upregulation of several immune-related Hallmark pathways, including *Complement*, *TNFα Signalling via NFκB* and *Inflammatory Response* in control animals (Figs. 5D and **S5**C). Importantly, T2D mice displayed comparable positive enrichment in response to infection in the same pathways as controls (Figs. 5D and **S5**C), suggesting that they mount similar immune responses. In line with this and the establishment of inflammatory foci following infection (Fig. 1K-M), we found no differences in gene expression of the pan-immune cell marker *Ptprc* (CD45) between T2D and control kidneys (**Figure S5**D). Similarly, macrophages, which form the first line of defence during *C. albicans* infection[37,38], were present at comparable levels in infected T2D and control animals (Figs. 5E-F and **S5**E), and we observed no differences in infection-induced cell death (a measure of inflammatory activation) of bone marrow-derived macrophages isolated from T2D and control mice (**Figure S5**F-G). We also considered neutrophils, which are rapidly recruited during *C. albicans* infection and play an important role in fungal killing[39]. We saw no evidence of defective neutrophil recruitment and expression of key effector enzymes, such as neutrophil elastase (NE) and myeloperoxidase (MPO), which were increased in T2D animals infected with *C. albicans* (Figs. 5G-I and **S5**H-J). In line with these findings and our proteomics and transcriptomics data, T2D and control mice also displayed comparable induction of IL-β transcript and protein with infection (**Figure S5**K-L), with IL-β being a key cytokine orchestrating the anti-*Candida* immune response[40]. Overall, these findings suggest that T2D mice are capable of mounting antifungal immune responses comparable to those observed in control mice.

Type 2 diabetic mice display stunted interferon and NK cell responses to C. albicans infection

Having established that T2D mice do not exhibit broad defects in anti-*Candida* responses, we considered that there may be nuanced dysregulation that might explain the increased fungal burden and disease severity. Our analyses identified numerous genes and proteins that were differentially expressed between T2Ds and controls both at baseline and following infection with *C. albicans* (Figs. 6A and **S6**A). While T2D animals showed higher expression of proteins and genes involved in *TNFα signalling via NFκB*, *Inflammatory Response* and *Complement* (Figs. 6B-C and **S6**B-C), we observed a significant deficit compared to controls in interferon (IFN)-alpha and -gamma responses, both at baseline and after infection (Figs. 6B and D and **S6**B and D). IFN-γ plays a central role not only in the establishment of protective T_H1-mediated adaptive immune responses to *Candida*, but also in boosting the phagocytic

and fungicidal capacity of macrophages and neutrophils[41]. Although IFN-γ can be produced by various immune cells, including T_H1 CD4 and CD8 T cells, natural killer (NK) cells are the most likely source at this early time point (24 hours post-infection). In line with this, we saw significantly reduced NK cell gene signatures in T2D mice compared to controls, both at baseline and after infection, in our kidney transcriptomics dataset, a result we were able to replicate in an independent 24-hour infection cohort using qPCR (Figs. 6E and **S6**E). Similarly, T2D mice displayed consistently lower expression of NK cell genes during the survival study (**Figure S6**F), independent of when the humane endpoint was reached. These results suggest that the deficit in IFN-γ signalling observed in T2D mice may directly result from reduced NK cell responses.

We also considered functional consequences of reduced IFN-γ signalling. IFN-γ plays an important role in upregulating antigen presentation, and T2D mice displayed a significant defect in protein and gene expression related to antigen presentation on both major histocompatibility (MHC) class I and class II complexes (Figs. 6F and **S6**G). Immunohistochemistry staining for MHC-II in infected kidneys further confirmed lower expression in T2D compared to control animals (Figs. 6G and **S6**H-I). MHC-II expression is not only important in the establishment of adaptive immune responses but can also serve as a proxy for the activation status of innate immune cells that are central to the anti-*Candida* response, such as macrophages and, to a lesser extent, neutrophils. Thus, we analysed kidney histology sections from the survival cohort to assess the ability of the immune response to contain and clear *C. albicans*. In control animals, *C. albicans* hyphae and diffuse immune cell recruitment were observed early during the infection (2–3 dpi) (Figs. 6H-I and **S6**J-L). From 4 dpi onwards, *C. albicans* hyphae were seen either surrounded by a ring of immune cells or were no longer visible within inflammatory foci of control animals (Figs. 6H-I and **S6**J-L). This indicates that control animals were able to contain and clear the infection. In contrast, T2D animals showed no signs of containment of the infection and still had visible hyphae at 5 dpi (Figs. 6H-I and **S6**J-L). Similarly, immunofluorescence staining for neutrophil extracellular traps (NETs) at 4 dpi revealed co-localisation of MPO and citrullinated histone H3 (H3Cit), indicative of NETs, around the edges of inflammatory foci in control animals, conveying containment, whereas NET staining was diffuse in T2D animals (Fig. 6J). Overall, our data indicate that T2D animals have deficits in important IFN-γ-mediated immune responses and show an inability to contain and clear *C. albicans*, ultimately resulting in aggravated disease pathology and worse survival.

DISCUSSION

In this study, we performed detailed characterisation of *C. albicans* infection in type 2 diabetes (T2D), whose incidence is projected to rise to close to 900 million by 2050, making it one of the fastest-growing global health threats of the 21st century[18]. It is increasingly recognised that there are subtypes of T2D with diverse aetiologies[42]. Thus, we used diverse mouse models that replicate genetic and dietary/obesity-associated T2D[43], which showed that, albeit varied, worsened disease outcomes of *C. albicans* infection are a common feature of T2D. Our study shows that a confluence of host and pathogen factors explains exacerbated fungal disease and mortality in T2D: long-term hyperglycaemia,

obesity and an associated metabolic dysfunction give rise to an imbalanced immune response defined by deficient interferon and NK cell signatures and higher pro-inflammatory responses. Coupled with the nutritional advantage provided to *C. albicans* by the glucose-rich environment, dysregulated immunity leads to an inability of the T2D host to mount organised immune responses to contain and clear the infection.

Increased susceptibility of diabetic hosts to infection, including bacterial and viral, is often attributed directly to high glucose levels. For example, studies have reported worse infection with bacterial or viral pathogens due to the effects of high glucose on host immune cell or physiological dysfunction[44–47]. High glucose levels have also been shown to increase pathogen growth or virulence[48,49]. Many of these studies concluded that normalising blood glucose levels may be sufficient to mitigate any negative effects of diabetes[45,47,49], and normalising blood glucose levels was sufficient to reduce skin infection with *C. albicans* in a mouse model of T1D (available as preprint[30]). Our data paint a more complex picture in bloodstream *C. albicans* infection in T2D, whereby glucose levels at the time of infection do not determine infection outcomes.

Specifically, while we provide evidence that *C. albicans* responds to and exploits high glucose availability at infection sites by upregulating glycolysis via transcription factors Tye7 and Gal4 to fuel its growth, blood glucose levels at the time of infection did not predict disease outcome. Moreover, lowering blood glucose levels with the SGLT2 inhibitor EMPA did not improve disease outcomes in T2D animals with *C. albicans* infection. We acknowledge we did not achieve complete normalisation of blood glucose levels with EMPA in our models of chronically hyperglycaemic and obese animals. Nevertheless, blood glucose was substantially and significantly lower with EMPA treatment, yet this made no difference to kidney fungal burden or serum levels of GDF15, a sensitive marker of disease severity. Seemingly contrasting with our data, a previous study in a mouse model of T1D showed that lowering glucose levels with thymoquinone led to reduced tissue fungal burden and improved survival of bloodstream *C. albicans* infection[29]. However, in that same study, lowering blood glucose with metformin had a much smaller effect on improving survival[29]. The findings with metformin support our findings with EMPA in our T2D model, and suggest that thymoquinone had effects on animal survival that were additional to lowering blood glucose levels. In line with our conclusions that hyperglycaemia *per se* is not the major determinant of worse infection outcomes, a recent study of *Streptococcus pneumoniae* lung infection showed that an acute increase in blood glucose levels by streptozotocin treatment of otherwise healthy mice does not lead to increased bacterial tissue burden[50]. Based on our findings, we conclude that chronic metabolic dysfunction in poorly controlled T2D, rather than glucose levels *per se*, drives poor outcomes of systemic *C. albicans* infection.

Our HFD model successfully uncoupled overt hyperglycaemia from obesity, showing that obesity, independently of overt hyperglycaemia, worsens outcomes of bloodstream *C. albicans* infection. Comparison of obese animals with the db/db animals that are both overtly hyperglycaemic and obese showed that combined overt hyperglycaemia and obesity further exacerbate *C. albicans* disease. Little is

known about obesity and *Candida* infection in human patients, but some studies have shown poor disease outcomes in obese patients infected with *C. albicans* or *C. auris*[51,52]. However, these same patients also had other health issues, such as neutropenia or COVID-19 infection, making it hard to directly attribute outcomes to obesity. In our experiments, animals fed a HFD became obese without confounding comorbidities, showing directly that obesity alone worsens outcomes of bloodstream *C. albicans* infection. Given that increasing numbers of people are eating poorly, and unhealthy body weight and obesity are prevalent, in-depth exploration of the mechanisms by which obesity impacts fungal disease is a key area for future research. Notably, obesity and T2D are not only diseases of impaired glucoregulation but are also marked by dysregulation of certain hormones and other metabolites such as lipids and amino acids[53,54]. Indeed, the levels of certain metabolites (glucose, raffinose, amino acids; **Fig. 3**) and several proteins involved in diverse aspects of metabolism (e.g. BCAT1, UGT1A1/3/9, BHMT, CYP7B1, CYP4A14, GSTA2, KYNU; https://github.com/hstoelting/CanDi) are basally altered in kidneys of T2D mice. Determining the mechanisms linking these factors to infection outcomes in chronic metabolic disease is an important question for future studies.

Our multi-omics and histology in *C. albicans*-infected kidneys demonstrated that T2D hosts mount antifungal immunity but are unable to clear infection. In-depth analyses showed dysregulated antifungal immunity in T2D hosts, with a hyperinflammatory phenotype accompanied by lower interferon and NK cell signatures and lower MHC-II expression. By simultaneously promoting tissue-damaging inflammation and crippling IFN-γ/NK cell–mediated pathogen control, this immune state creates a dual pathway for disease progression [41,55–57]. Neutrophils are the key immune cell type for killing *C. albicans*, and their antifungal effector functions depend on glucose availability[9]. Our data show that key neutrophil effector enzymes, NE and MPO, are increased in *C. albicans*-infected T2D kidneys, but NETs fail to organise around *C. albicans* infection foci to contain fungal growth. Our results contrast with earlier work showing that neutrophils isolated from T1D rats displayed decreased phagocytosis and killing of *C. albicans*[58] and the reported reduced killing of *C. albicans* by neutrophils from diabetic patients[59]. However, our findings are supported by studies showing increased NETosis in neutrophils from type 1 and type 2 diabetic patients and animals[60,61], although another study suggested that high glucose levels, which are sufficient to trigger NETosis on their own, may impair NETosis in response to LPS stimulation[62]. Taken together, our findings and these previous studies show a key impact of metabolic context on neutrophil functions. However, regardless of increased or decreased effector functions, diabetes impairs the ability of neutrophils to control pathogens even when effector functions, such as NETosis, are increased.

Further supporting our findings, exacerbated pro-inflammatory cytokine responses (or ‘cytokine storm’) such as those observed in T2D mice have been linked to multi-organ failure and mortality during severe infections with pathogens of all classes[63,64]. In COVID-19, aggravated morbidity and mortality of patients with T2D, particularly those with poor glycaemic control, is thought to be related to exacerbated inflammation compared to non-diabetic people[65–67]. High IL-6 levels, such as observed in T2D kidneys (https://github.com/hstoelting/CanDi), have also been postulated to predict mortality in candidaemia[68].

At the same time, there are reports of lower serum IFN-γ levels and a reduced ability of circulating immune cells to produce IFN-γ in patients with T2D[44,69–73], with fewer reports of elevated IFN-γ in T2D[74,75]. Murine models of bloodstream *C. albicans* infection also showed lower IFN-γ levels in T1D animals, together with reduced fungal phagocytosis by splenic macrophages and a proposed shift from an antifungal Th1 immune response to an ill-suited Th2 response[23,24]. Providing further support to our findings, recent peer-reviewed[76] and preprint[77] studies found reduced *Interferon Gamma Signalling* signatures in monocytes from T2D db/db mice and T2D patients, and NK cell deficiencies have also been reported in diabetes[78–80]. Given the timeline of our experiments (endpoint at 24 hours after infection), NK cells are a likely source of IFN-γ in our model. Similarly, bacterial lung infection with *Legionella pneumophila* or *Streptococcus pneumoniae* in mouse models of T2D (including db/db and HFD-fed mice) showed lower IFN-γ production by NK cells to be responsible for immune failure to control infection[50]. In addition to producing cytokines, NK cells also display direct fungicidal activity[56,81,82]. One of the NK cell receptors important for recognising and killing *C. albicans*, NKG2D (encoded by *Klrk1*)[56] was expressed at significantly lower levels in kidneys of T2D animals in our model (Fig. 6E). Recent work showed that genetic or antibody-based blockade of NKG2D renders mice hypersusceptible to bloodstream *C. albicans* infection[56], showing how low NKG2D levels in diabetes could contribute to poor *C. albicans* control. Collectively, these findings suggest that the defective IFN-γ and NK cell signatures that we found in the T2D animals impair the ability of immune cells to organise, contain and clear *C. albicans*.

Our study shows that long-term glycaemic control and metabolic health are important for effective antifungal immunity that enables early control of fungal growth, before *C. albicans* takes advantage of high glucose levels in T2D tissues to supercharge its own growth and cause hyperinflammation and mortality. Consistently, immune cell dysfunction has been reported in poorly controlled relative to well-controlled T2D subjects[44,70]. Our findings have implications for patients with poorly controlled diabetes, for whom acute lowering of glucose levels, while important, may not be sufficient to improve *C. albicans* infection outcomes. It should also be considered that *C. albicans* infection *per se* perturbs glycaemic control and causes a reduction in blood glucose levels in both control and T2D animals[7,83]. Immune responses and pathogens alike rely on glycolysis, and metformin treatment caused severe hypoglycaemia and worse outcomes in *C. albicans*-infected non-T2D mice[7]. Therefore, in addition to normalising glucose levels, there may also be scope for immunotherapies and nutritional interventions in T2D patients, such as providing glycine, as a 30-day glycine trial in T2D patients helped with glycaemic control and boosted IFN-γ responses while keeping TNFR1 signalling in check[84].

In conclusion, our study provides an in-depth understanding of fungal pathogen and host responses in the context of T2D and obesity, disentangling the mechanistic effects of overt hyperglycaemia and obesity on pathogen growth and immune responses, and suggesting that long-term glycaemic control to reduce metabolic dysfunction, rather than acute glucose control, is critical for surviving bloodstream *C. albicans* infection. Our multi-omics data of host responses in *C. albicans* infection environments in T2D

and control hosts, as well as our custom-made *CanDi* viewer (https://github.com/hstoelting/CanDi) to promote interactive data exploration, provide a rich resource for understanding host responses to a major human pathogen in health and metabolic diseases.

STUDY LIMITATIONS

The bloodstream (intravenous) infection model of *C. albicans* that we have used leads to disseminated disease, whereby kidneys are the primary site of fungal growth. In this model, the *C. albicans* inoculum is given directly into the bloodstream. This is a gold standard in the field for inducing systemic infection, mimicking disease in hospitalised patients caused by contamination of medical devices, chiefly central venous catheters[85]. Disease can be caused by a range of *C. albicans* strains, and patients are thought to be infected by their own commensal strain[86]. We used the prototype *C. albicans* strain SC5314, and future studies should address different fungal strains. On the host side, our experiments show that both male and female T2D (db/db) animals are more susceptible to *C. albicans* infection, while our multi-omics, NZO and HFD models used only male mice. While T2D is most commonly seen in older adults, we used relatively young mice. The comprehensive effects of sex and age on infection susceptibility in T2D are important questions for future studies.

METHODS

Candida albicans strains and growth conditions

The *C. albicans* strains used in this study were the clinical isolate SC5314, CAS9 (tye7Δ::FRT/tye7Δ::FRT, gal4Δ::ARG4/gal4Δ::HIS1, RPS10/rps10::URA3)[6] and CAS10 (tye7Δ::FRT/TYE7::FRT, gal4Δ::ARG4/GAL4::FRT, HIS1/his1::hisG, RPS10/rps10::URA3)[6]. Unless stated otherwise, SC5314 was used for experiments. Frozen stocks were streaked onto YPD (1% yeast extract, 2% peptone, 2% glucose, 80 µg/ml uridine) agar (2%) plates and grown at 30°C for three days. Liquid cultures were prepared by resuspending a single colony from a plate culture in 5 ml of YPD liquid medium and incubating at 30°C with shaking at 200 rpm overnight (~ 16 hours).

Animal experiments

Ethics and monitoring

All animal procedures were conducted in accordance with the NHMRC Australian Code of Practice for the Care and Use of Animals and were approved by the Monash University Animal Ethics Committee (MUAEC)-2 (Approval Number: 41762). Animals were monitored at least once per week before infection or twice daily during infection experiments for body weight changes and clinical signs of illness and were euthanised if they reached humane endpoints (score of 1 in 3 or more categories or score of 2 in any category; **Table S1**).

Mouse strains and husbandry

BKS.Cg-Dock7m +/+ Leprdb/J (db/db) and New Zealand Obese (NZO), originally sourced from The Jackson Laboratory (JAX strains #000642 and #002105), were derived from internal colonies bred and housed within the Monash Animal Research Platform (MARP). Both strains were maintained on highly absorbent Fibrecycle bedding, and cages were changed three times per week due to the increased urinary output of T2D animals. Male wildtype C57BL/6J animals were purchased from MARP (C57BL/6JMARP) and maintained on regular sawdust bedding with weekly cage changes. All animals were housed in Optimice individually ventilated cage (IVC) systems (Animal Care Systems, Centennial, CO, USA) before and during experiments, with a maximum occupancy of three (db/db and NZO) or five (C57BL/6JMARP) mice per cage and kept on a 12-hour light/12-hour dark cycle. Animals were given *ad libitum* access to food and water, and unless stated otherwise, db/db mice and NZO mice were fed a 4.2%-fat chow diet (SF00-100, Specialty Feeds, Glen Forrest, WA, Australia) and C57BL/6JMARP mice were fed an 8.5%-fat chow diet (Barastoc Research Feeds Mouse Breeder Cube, Ridley AgriProducts).

Where food intake was measured (cohort 2 of db/db survival experiment, cohort 1 and 2 of HFD-induced obesity endpoint study, NZO experiment and db/db empagliflozin experiment), mice were singly housed in individual compartments of divided Optimice cages (two animals per cage) at least three days prior to infection to allow for acclimatisation to single housing and measurement of baseline food intake. Food hopper contents of each animal were weighed up to twice a day during standard monitoring.

High-fat diet-induced obesity

To induce obesity, 7-week-old male C57BL/6JMARP mice were placed on a semi-pure 34.5%-fat diet (SF13-092, Speciality Feeds; hereafter referred to as high-fat diet, HFD) for 13 or 16 weeks, until they reached at least 42 g of body weight. Control mice were maintained on the standard 8.5%-fat chow diet (Barastoc Research Feeds Mouse Breeder Cube).

New Zealand Obese (NZO) model

To accelerate onset of hyperglycaemia, male NZO mice were placed on HFD at 8–11 weeks of age. Random-fed blood glucose levels were measured between 8 and 10 a.m. immediately before the diet swap and after 3, 5.5 and 7 weeks on the diet, by puncturing the lateral tail vein with a 27G needle to produce a drop of blood and measuring blood glucose using an Accu-Chek® hand-held glucometer (Roche Diabetes Care).

Empagliflozin treatment of db/db mice

Empagliflozin (AMBH2D6FA460) was purchased from Merck (Darmstadt, Germany). All diet preparation steps were performed within a Class II biological safety cabinet. 4.2%-fat chow diet (SF00-100) was pulverised using a Nutri Ninja Blender (BL642, SharkNinja). Empagliflozin powder (30 mg per 100 g dry diet weight to yield a final concentration of 0.03% w/w) was first mixed into a small amount of finely pulverised diet before stirring the resulting blend into the rest of the pulverised diet. Sterile water (25 ml

per 100 g dry diet weight) containing a few drops of food-safe dye was mixed in to form a thick paste. A scalpel was used to remove the needle hub of a 5-ml disposable syringe, and diet pellets were formed by compacting the diet paste within the barrel of the syringe and expelling it with the help of the plunger. The diet was then spread out on a tray within a running Class II biological safety cabinet and left to dry overnight before storage in airtight containers at 4°C for up to one week. The resulting pellets were slightly larger, softer and crumblier than the original chow diet. A control diet was prepared in the same manner, without the addition of drug.

11-14-week-old db/db mice of both sexes were placed on either the empagliflozin-containing or control diet 7 days prior to infection, and random-fed blood glucose measurements were taken as described above immediately before diet swap and after 3 and 6 days on the experimental diet.

Infection with C. albicans

To induce systemic *C. albicans* infection of mice, 1 ml of liquid culture was pelleted by centrifugation (5 min at 2500×*g*), washed three times in 1 ml of sterile PBS and manually counted using a disposable Neubauer counting chamber (INCYTO). The inoculum was diluted to a concentration of 1×10^6 CFU per ml in sterile PBS. The actual number of CFU within the infection inoculum was determined by plating dilutions on YPD plates, incubating for two days at 30°C and counting colonies. Mice were warmed under a heat lamp for 5 to 10 minutes and then injected with 100 µl of inoculum (containing 1×10^5 CFU *C. albicans*) intravenously into the lateral tail vein. Uninfected controls received sterile PBS instead. Unless stated otherwise, mice were culled and tissues harvested at 24 hours post-infection.

Euthanasia and organ collection

Upon reaching the experimental or humane endpoint, mice were culled by cervical dislocation, followed by immediate decapitation. Trunk blood was collected on parafilm squares prior to blood glucose measurement using a hand-held glucometer and transfer into microfuge tubes on ice. Organs were removed and processed and/or stored according to downstream analyses.

Colony-forming unit (CFU) assay

Right kidneys and spleens were collected in 2 ml of sterile PBS containing Complete EDTA-free Protease Inhibitor (Roche) and 0.05% Tween-20 and stored on ice before homogenisation using a Tissue Master 125 homogeniser (Revvity). Tissue weights were recorded by weighing homogenisation tubes before and after addition of tissues. Homogenates were serially diluted, plated on YPD agar plates containing 50 µg/ml of ampicillin and incubated at 30°C for two days. CFU plates were photographed and colonies manually counted. Results are expressed as CFU per right kidney or CFU/g of kidney. Where two strains were used in the same experiment, results were adjusted for the actual concentration in the infection inoculum as determined by plating.

Histology, staining, image acquisition and analysis

Tissue processing and standard histology stains

Left kidneys were halved longitudinally and one half fixed by submersion in 10% neutral-buffered formalin for at least 24 hours. Tissues were paraffin-embedded and sectioned at a thickness of 4 µm for haematoxylin and eosin (H&E), periodic acid-Schiff (PAS), immunohistochemistry (IHC) and immunofluorescence staining. Tissue embedding, sectioning and standard histological stains (H&E, PAS) were performed by the Monash Histology Platform at Monash University.

Immunohistochemistry

IHC staining was performed by the Monash Histology Platform. Kidney sections were dewaxed and rehydrated prior to heat-induced antigen retrieval in citrate pH 6.1 (Dako S1699, Agilent; F4/80) or 10 mM Tris-EDTA pH 9.0 (MHC Class II) target retrieval buffer for 30 min at 98°C. Sections were washed in Dako EnVision FLEX wash buffer (Agilent) for 5 min at room temperature and sequentially blocked with Dako REAL Peroxidase-Blocking Solution and serum-free protein block (both Dako, Agilent) at room temperature for 10 min each. Sections were then stained with primary antibodies against F4/80 (1.1 µg/ml, clone D2S95, rabbit monoclonal antibody, Cell Signaling Technology) or MHC Class II (I-A/I-E; 10 µg/ml, clone M5/114.15.2, rat monoclonal antibody, Invitrogen) for 60 min at room temperature. Following a 5-min wash in wash buffer, sections were incubated with HRP-conjugated secondary antibodies raised against rabbit (Dako, EnVision+/HRP, Rabbit, K4003, Agilent) or rat (2 µg/ml, goat polyclonal IgG, ab205720, abcam) for 30 min at room temperature. Following three additional washes, slides were incubated with Dako DAB+ Substrate (Agilent) for 10 min at room temperature, rinsed with the appropriate wash buffer (Dako K3468) and incubated with Dako Ready-to-use Hematoxylin (Agilent) for 5 min at room temperature. Following two rinses in distilled water, slides were dehydrated, cleared in xylene and mounted using Leica CV Mount medium (Leica Biosystems).

Immunofluorescence

Sections were dewaxed, rehydrated, and incubated in antigen retrieval buffer (10 mM Tris, 1 mM EDTA, pH 9) in a pressure cooker for 10 min. Slides were blocked in PBS containing 10% chicken sera and 5% BSA for 30 min at room temperature and probed with antibodies against MPO (10 µg/ml, goat polyclonal, AF3667, R&D Systems) and citrullinated histone H3 (20 µg/ml, rabbit polyclonal IgG, ab5103, abcam) diluted in PBS containing 1% bovine serum and 5% BSA for 16 hours at 4°C. Rabbit and goat Ig were used as isotype controls (purified from whole serum from Sigma). Sections were then incubated with fluorophore-conjugated secondary antibodies raised against goat (10 µg/ml, chicken polyclonal IgY, AlexaFluor™ 594, A-21468, Thermo Fisher Scientific) or rabbit (10 µg/ml, chicken polyclonal IgY, AlexaFluor™ 488, A-21441, Thermo Fisher Scientific) for 40 min at room temperature. To quench tissue autofluorescence, slides were incubated with Sudan Black B (0.1% in 70% ethanol) for 30 min at room temperature, washed in PBS, and mounted in DAPI ProLong Gold (Thermo Fisher Scientific).

Image acquisition and analysis

Images of H&E-, PAS- or IHC-stained sections were acquired using an Aperio ScanScope AT Turbo or Aperio GT450 (both Leica Biosystems) slide scanning system at 20x apparent magnification.

Whole-slide immunofluorescence imaging was performed using an Olympus VS200 research slide scanner equipped with an Excelitas X-Cite XYLIS LED light source and a Hamamatsu ORCA-Flash4.0 sCMOS camera. Images were acquired using an Olympus UPLXAPO 20× objective lens. Fluorescence was excited using the appropriate LED wavelength band (DAPI, FITC for AF488 and mCherry for AF594) and captured using 432/36 nm (DAPI), 474/27 (FITC/AF488) and 578/21 nm (mCherry/AF594) emission filters.

Image analysis of whole tissue sections was conducted using QuPath software (version 0.6.0[87]). Threshold-based pixel classifiers were built within QuPath to segment total tissue areas, inflammatory foci (H&E and PAS), fungal hyphae (PAS), and positively stained areas in IHC- and IF-stained sections. For all tissue sections, a threshold-based pixel classifier operating at very low resolution was used to annotate the total tissue area (minimum object size: 5,000,000 μm^2 for brightfield images and 1,500,000 μm^2 for fluorescence images; minimum hole size: 15,000 μm^2 for brightfield images and 50,000 μm^2 for fluorescence images). On H&E- and PAS-stained sections, inflammatory foci were identified using a very low-resolution threshold classifier targeting the Haematoxylin signal (minimum object size: 7,500 μm^2; minimum hole size: 7,500 μm^2). False-positive detections (e.g., caused by smudges) were manually removed. Fungal hyphae on PAS-stained sections were segmented at full resolution using a threshold classifier applied to the PAS signal (minimum area: 10 μm^2; minimum hole size: 0 μm^2). False-positive detections caused by tissue background were manually removed. For DAB-stained IHC images, positive signal detection was performed at full resolution using a DAB-specific threshold classifier (minimum object size: 10 μm^2). MPO-positive areas in IF images were defined using an AF594-specific threshold classifier (minimum object size: 100 μm^2; minimum hole size: 50 μm^2). Detection results were expressed as area relative to total tissue area or area of inflammatory foci.

Representative images were exported using QuPath, and scale bars were embedded using Fiji software (version 2.14.0/1.54f[88]). For immunofluorescence images, Fiji software was used to apply pseudo-colours and adjust minimum and maximum display values for optimal visualisation. Colour deconvolution of PAS images was performed using the Fiji built-in *Color Deconvolution* plug-in[89] with a custom user-defined stain vector matrix calibrated to the experimental samples [Stain 1 (Haematoxylin): R = 0.651, G = 0.701, B = 0.290; Stain 2 (PAS): R = 0.279, G = 0.878, B = 0.389; Stain 3 (Residual): R = 0.043, G = -0.416, B = 0.908] to separate colour components into distinct channel images for downstream visualisation. Blue and Fire pseudo-colour lookup tables were assigned to the haematoxylin and PAS signal, respectively, and images were remerged for presentation.

RNA isolation, cDNA synthesis and qPCR

RNA isolation

Unless stated otherwise, snap-frozen kidney pieces weighing around 15–25 mg were added to 2 ml microcentrifuge tubes containing 1 mm zirconia beads (BioSpec) and 0.5 ml of RNAzol RT reagent (Sigma) and homogenised in a CryoMill Cryogenic Mixer (Retsch) (2×2 min at 30 Hz). To break up fungal

cell walls, the resultant homogenates were transferred into fresh 2ml microcentrifuge tubes containing 425–600 µm acid-washed glass beads (Sigma) and subjected to one more round of homogenisation on the CryoMill (1×2 min at 30 Hz). Total RNA was then isolated according to the manufacturer's instructions for the RNAzol RT reagent. Briefly, 0.2 ml of RNase-free water was added to each sample, samples were vortexed for 15 s, left to stand for 15 min and then centrifuged for 15 minutes at 12,000×*g* and 4°C. 450 µl of the resulting supernatants were transferred to fresh microcentrifuge tubes, equal volumes of 100% isopropanol were added, samples were vortexed, left to stand for 10 minutes and centrifuged for 10 minutes at 12,000×*g* at room temperature. Supernatants were discarded, and RNA pellets were washed twice with 250 µl of 75% ethanol (v/v) with 2-min centrifugation steps at 6,000×*g* and room temperature between washes. Washed pellets were immediately solubilised in 50 µl of RNA-free water and vortexed or shaken for 2 to 5 minutes before measurement of RNA concentrations using a spectrophotometer.

cDNA synthesis and qPCR

Up to 1 µg of RNA was transcribed into cDNA using the LunaScript RT SuperMix Kit (New England Biolabs) according to manufacturer's recommendations. cDNA was diluted using RNase-free water prior to qPCR analysis. Gene expression was analysed using custom primer pairs (**Table S2**) and QuantiNova SYBR Green reagents (Qiagen) on a QuantStudio 5 RealTime PCR machine (Thermo Fisher Scientific). Gene expression was calculated relative to that of the murine housekeeping gene *Tbp*. To correct for differences in pathogen load, fungal genes were normalised to expression of fungal *18S* and *RDN25*.

Serum collection and biochemical assays

Serum was collected following centrifugation of blood samples at 8,000×*g* for 10 min at 4°C. Levels of alanine aminotransferase (ALT), aspartate aminotransferase (AST) and creatinine were measured using Indiko Clinical Chemistry reagents (Thermo Fisher Scientific).

For ALT and AST measurements using the IFCC method, working reagents were prepared by combining Reagents A and B. 2 µl of serum samples or water (blank) were pipetted into wells of a UV-grade 96-well plate (Corning). 100 µl of working reagent was added to each well immediately before measuring absorbance at 340 nm every 60 seconds for a total of 30 min using a CLARIOStar Plus plate reader (BMG LabTech) set to 37°C. MARS software (version 3.32) was used to calculate the slope during the linear stage decline of absorbance at 340 nm. ALT and AST activity in U/L were calculated using the following formula: $Activity\ (sample) = \frac{\Delta\ Abs \times\ 2.603 \times\ 10^4\ \mu\ M}{Time\ (mins)}$, based on the assumptions that 1 *U* of enzyme converts 1 µmol of NADH per minute and that the concentration of NADH in the well can be calculated as $Concentration\ = \frac{Abs}{Molar\ extinction\ coefficient\ (NADH) \times\ Path\ length}$, with the molar extinction coefficient of NADH being $6.3 \times 10^3\ M^{-1}\ cm^{-1}$, the path length estimated at 0.311 cm, and the activity of the sample adjusted for the 51-fold dilution in the reaction.

Creatinine levels were determined using the Jaffé method. Working reagent was prepared by combining Reagents A and B. 7.5 µl of serum samples or water (blank) were pipetted into wells of a half-area clear

flat-bottom 96-well plate (Corning). A 7-point standard curve was prepared by 2-fold dilutions of 20 µg/ml creatinine (Sigma) in water (range: 0.3125-20 µg/ml). The assay was confirmed to be highly linear in this range (R^2 = 0.9997). 50 µl of working reagent was added to each well, and absorbance at 510 nm was measured immediately and again after 5 min using an Infinite 200 plate reader (Tecan). The change in absorbance over the assay period was calculated for all samples and standards, and sample concentrations were determined through interpolation from the linear standard curve.

ELISA

Mouse DuoSet ELISA kits (R&D Systems) were used according to the manufacturer's instructions to measure GDF15 in serum samples and IL-1β in kidney homogenates generated for CFU determination, which were cleared by centrifugation at 3,000×*g* for 5 min prior to analysis.

Kidney glucose measurement

Snap-frozen kidney pieces (~ 15 mg) were weighed, placed inside 2 ml microcentrifuge tubes containing a 5 mm stainless steel bead kept on ice, and 1 ml of pre-chilled Homogenisation Buffer (50 mM Tris, pH 7.5) and 125 µl of pre-chilled Inactivation Solution (0.6 N HCl) were added. Tissues were homogenised in a CryoMill Cryogenic mixer for 2 min at 30 Hz, 125 µl of Neutralisation Solution (1 M Tris base) was added, and samples were centrifuged at 3,000×*g* and 4°C for 5 min. Cleared lysates were transferred to fresh microcentrifuge tubes and stored at -20°C or analysed immediately. A sample dilution buffer was prepared by mixing Homogenisation Buffer, Inactivation Solution and Neutralisation Solution at an 8:1:1 ratio. A 7-point standard curve was prepared through 2-fold serial dilution of 1 mg/ml glucose in dilution buffer (range: 15.625–1000 µg/ml). 20 µl of undiluted sample, standard or blank (dilution buffer) was pipetted into a UV-grade flat-bottom 96-well plate (Corning). A working reagent was prepared by combining reagents A and B of the Indiko Glucose (HK) clinical chemistry reagents (Thermo Fisher Scientific). 200 µl of working reagent was added to each well, and plates were incubated for 10 min at room temperature prior to reading the absorbance at 340 nm once per min for 20 min. To calculate glucose tissue concentration, absorbance values were averaged across measurements, blank-corrected, and concentrations interpolated from the standard curve through linear regression. Concentrations were corrected for buffer volume and tissue weight and expressed as mg of glucose per g of kidney.

Candida infection and live-cell imaging of bone marrow-derived macrophages

Bone marrow was collected from 13-week-old db/db and control mice as previously described[90]. Body weights and blood glucose levels were also recorded. Briefly, femurs and tibias were dissected, cleaned of any fat, muscle and connective tissues and kept in RPMI containing 10% foetal bovine serum (FBS), penicillin (100 U/ml) and streptomycin (100 µg/ml; P/S) and 12.5 mM HEPES (cRPMI) at 4°C until further processing. Bones were cut open on both sides and placed into a 0.5 ml microcentrifuge tube with a small hole in the bottom and nested inside a 1.5 ml microcentrifuge tube. Samples were centrifuged at 10,000×*g* for 15–30 s, cleared bones were discarded, and bone marrow pellets were resuspended in cRPMI. Bone marrow cells were plated in T25 flasks in 5 ml of cRPMI and incubated overnight at 37°C

and 5% CO_2. The following day, supernatants were collected, centrifuged at 300×*g* for 5 min and resuspended in FBS containing 10% DMSO and aliquoted into cryovials for storage.

Bone marrow-derived macrophage (BMDM) medium was prepared from RPMI containing 12.5 mM HEPES, 20% L-Cell conditioned media, 15% FBS and P/S. Bone marrow cells were thawed, resuspended in BMDM medium, plated on 10 cm Petri dishes and cultured for 7 days at 37°C and 5% CO_2. To harvest BMDMs, cells were gently scraped in cold PBS, centrifuged for 5 min at 450×*g*, resuspended in BMDM medium and plated in a 96-well plate at 1×10^5 cells per well in 100 µl. The following day, the medium was replaced with 1 µM CellTracker Green (CTG; Thermo Fisher Scientific) in 100 µl of serum-free RPMI containing 12.5 mM HEPES and P/S. Cells were incubated for 30 min at 37°C and 5% CO_2. In the meantime, a fungal inoculum containing 3×10^6 CFU of *C. albicans* SC5314 per ml of BMDM medium was prepared from a liquid overnight culture as described above. CTG was replaced with 100 µl of fungal inoculum (MOI 3) or BMDM medium, and cells were incubated for 1 hour at 37°C and 5% CO_2. Cells were gently washed with PBS three times to remove extracellular yeast cells, and 150 µl of BMDM medium containing 0.6 µM of DRAQ7 (Abcam) was added to each well.

Cells were imaged once every 30 min for 24 hours at 37°C and 5% CO_2 using a Leica AF6000 LX epifluorescence microscope equipped with a 20× objective lens (Leica Biosystems). Image analysis was conducted in *CellProfiler* (version 4.2.8[91]). Total cell counts were determined by inverting brightfield images, calculating and correcting illumination, rescaling intensity and identifying primary objects in the first frame. Dead ($DRAQ7^+$) cells were counted in all frames by rescaling intensity and identifying primary objects. If the number of $DRAQ7^+$ cells in any frame exceeded the number of total cells counted in the first frame, that number was used as the total number of cells in the downstream analysis. Macrophage cell death over time was expressed as the percentage of $DRAQ7^+$ cells of total cells.

Transcriptomics analysis of kidney homogenates

RNA isolation

For samples used for transcriptomics, RNA was isolated using a combination of RNAzol RT reagent and the RNeasy Plus Mini extraction kit (Qiagen). Briefly, following the first centrifugation step after homogenisation in RNAzol and addition of water (described above under RNA isolation, cDNA synthesis and qPCR), 350 µl of supernatant was added to gDNA eliminator columns, and RNA was extracted according to the manufacturer's protocol for the RNeasy Plus Mini kit. RNA quality was determined by running a Eukaryote Total RNA Nano assay on an Agilent 2100 Bioanalyzer, with RNA Integrity Numbers (RIN) of 7.6 or higher for all samples.

Library preparation and sequencing

Sequencing libraries were prepared using the Illumina Stranded mRNA Prep kit (Illumina), which enriches for polyadenylated transcripts via poly(A) selection prior to fragmentation and strand-specific cDNA synthesis. For each sample, 600–900 ng of total RNA was used as starting material. Libraries were

sequenced by Novogene (Novogene Co., Ltd.) on an Illumina NovaSeq X Plus platform using a paired-end 150 bp (PE150) sequencing configuration, with a target depth of approximately 20 million paired-end reads per sample and demultiplexed FASTQ files were provided for each sample.

Data analysis

Raw paired-end Illumina sequencing reads (2×150 bp) were assessed for quality using *FastQC* (version 0.12.1) compiled via *MultiQC* (version 1.32). Read evaluation confirmed high sequence quality across all samples (mean Phred score > 35 across the entire read length, acceptable GC content, optimal per-base sequence quality and length distribution). Sequence alignment and determination of gene-level read counts were performed on the M3 High-Performance Computing (HPC) cluster (Monash University). Reference genomes and annotation files for mouse (*Mus musculus*, GRCm39 / GCF_000001635.27) and *Candida albicans* (ASM18296v3 / GCF_000182965.3) were retrieved from the NCBI database (https://ftp.ncbi.nlm.nih.gov/genomes/refseq/), and genome indices were constructed using *Minimap2* (version 2.28). Alignment was performed sequentially, with paired-end reads first being aligned to the mouse reference using *Minimap2* (-a -x sr). *Samtools* (version 1.19.3) was used to sort the resulting SAM files and convert them to coordinate-sorted BAM files for gene quantification. To isolate fungal transcripts, name-sorted BAM files were generated to extract unmapped read pairs, which were converted back to FASTQ format and subsequently aligned to the *C. albicans* reference genome using identical parameters.

Read counts were quantified from coordinate-sorted BAM files using *featureCounts* from the *Subread* package (version 2.0.1). Libraries were designated as reverse-stranded (-s 2), paired-end (-p), with read overlap permitted across multiple features (-o). For mouse transcripts, features were grouped by *gene_id* at the exon level (-t exon) against the GRCm39 GTF annotation. A conservative minimum mapping quality score threshold was applied (-Q 10). For *C. albicans* transcripts, reads were mapped to the ASM18296v3 GTF annotation at gene level (-t gene) with no minimum mapping quality restrictions (-Q 0). Multi-mapping reads were assigned fractionally (-M --fraction). To prevent cross-hybridisation artifacts and false-positive pathogen signals in the dual RNA-seq analysis, alignment profiles of *C. albicans* genes with high read counts in uninfected samples were visually inspected using *Integrative Genomics Viewer* (IGV, version 2.19.8). A total of 8 *C. albicans* genes (CAALFM_CR08810WA, CAALFM_CR01530CA, CAALFM_C109070WA, CAALFM_C205090WA, CAALFM_CR09470WA, CAALFM_CR08770WA, CAALFM_CR08790WA, CAALFM_CR08760CA) were excluded due to either conserved region artifacts (read coverage restricted to a narrow span rather than distributed across the full-length transcript) or rRNA background (sequence homology between host and fungal rRNAs).

Downstream processing and statistical testing were performed in RStudio (version 2025.05.0 Build 496; R version 4.5.0). Mouse and *Candida* counts were analysed separately. For the analysis of mouse transcripts, low-abundance genes were removed by retaining only features with at least 10 raw counts in at least one sample. Compositional bias and library size variations were normalised using the Trimmed Mean of M-values (TMM) method in *edgeR* (version 4.6.2), followed by log-CPM transformation and precision weighting using the *limma* package (version 3.64.3). The *limma* package was also used to

perform differential gene expression analysis. Linear models were fitted to the transformed data across the four experimental groups, and pairwise comparisons of interest (Control/Candida vs Control/PBS, T2D/Candida vs T2D/PBS, T2D/PBS vs Control/PBS, T2D/Candida vs Control/Candida) were evaluated. Empirical Bayes moderation was applied to obtain moderated *t*-statistics and adjusted *p*-values (Benjamini-Hochberg false discovery rate, FDR). Sample relationships were visualised using multidimensional scaling (MDS) based on pairwise Pearson correlation distances ($d = 1 - r$), calculated via classic metric multidimensional scaling using the *stats* package (version 4.5.0). To perform Gene Set Enrichment Analysis (GSEA), Murine Hallmark gene sets (MH) were retrieved from the Molecular Signatures Database (MSigDB) using the *msigdbr* package (version 26.1.0). For each comparison, normalised enrichment scores and FDR-adjusted p-values were calculated based on fold change-ranked gene lists using the *clusterProfiler* package (version 4.16.0[92]). Pathways with an FDR < 0.05 were considered significantly enriched.

The analysis of *Candida* transcripts was restricted to genes with at least 5 raw counts in at least one sample, and only infected samples were included. Normalisation, transformation and differential gene expression analysis (T2D/Candida vs Control/Candida) were performed using *edgeR* and *limma* as described above.

Proteomics analysis of kidney homogenates

Tissue processing

Mouse kidney tissue (10–20 mg) was ground in a mortar and pestle with liquid nitrogen, then transferred to fresh 1.5 ml microcentrifuge tubes and resuspended in 300 µl of SDS lysis buffer (5% w/v sodium dodecyl sulphate, 100 mM HEPES, pH 8.1), heated at 95°C for 10 min and then probe-sonicated before measuring the protein concentration using the BCA method. A total of 50 µg of protein was denatured and alkylated by adding TCEP (Tris(2-carboxyethyl) phosphine hydrochloride) and CAA (2-Chloroacetamide) to a final concentration of 10 mM and 40 mM, respectively, and the mixture was incubated at 55°C for 15 min. Sequencing-grade trypsin (Promega) and LysC (FUJIFILM Wako) were added at an enzyme-to-protein ratio of 1:50 and incubated overnight at 37°C after the proteins were trapped using S-Trap mini columns (Protifi). Tryptic peptides were sequentially eluted from the columns using (i) 50 mM TEAB, (ii) 0.2% formic acid and (iii) 50% acetonitrile (ACN), 0.2% formic acid. The fractions were pooled and concentrated in a vacuum concentrator prior to peptide cleanup with solid-phase extraction using in-house packed SDB-RPS (Empore SDB-RPS C8; Merck, 14-386-8). Briefly, samples were loaded into the tips and centrifuged at 15,000×*g* for 7 min. Flowthrough was removed, and 100 µL of SDB-RPS Loading buffer (1% TFA in isopropanol) was loaded into the top of the tip and centrifuged again at 15,000×*g* for 7 min. Flowthrough was discarded, and the step was repeated twice. Then 100 µL of SDB-RPS Wash buffer (0.2% TFA /5% ACN) was loaded into the tip and centrifuged at 15,000×*g* for 7 min. Flowthrough was discarded, and the step was repeated twice. Peptides were eluted using 100 µL of SDB elution buffer (5% NH4OH in 60% ACN) and centrifuged at 15,000×*g* for 7 min in a fresh microcentrifuge tube. Eluates were vacuum centrifuged to dryness prior to reconstitution in 15 µL

of MS loading buffer (2% ACN, 0.1% TFA) with iRT peptides, then sonicated for 10 min in a water bath, and transferred into MS vials to be loaded into the mass spectrometer.

Liquid chromatography-mass spectrometry

Samples were analysed via liquid chromatography-mass spectrometry (LC-MS) using the Orbitrap Astral mass spectrometer (Thermo Fisher Scientific) coupled with a Vanquish Neo UHPLC system (Thermo Fisher Scientific) in direct injection mode on an Aurora® Elite™ 15×75 C18 UHPLC column (IonOpticks). A reversed-phase linear gradient was developed over 30 minutes from solvent A (0.1% formic acid in water) to 50% solvent B (80% ACN/ 0.1% formic acid), maintaining a flow rate of 0.4 µL/min. Electrospray ionisation (ESI) was performed with a static spray voltage of 1900 V in positive ion mode. The ion transfer tube was maintained at 300°C. MS raw files were uploaded to the PRIDE[93] partner repository with the dataset identifier PXD083872. The MS parameters were as follows: 100 ng of peptide was loaded onto the column. The Orbitrap Astral mass spectrometer was operated in data-independent acquisition (DIA) mode. Survey scans were acquired in the Orbitrap at a resolution of 240,000 with a scan range of 380–980 m/z. For the DIA analysis, precursor ions were fragmented using high-energy collision dissociation (HCD) with a normalised collision energy (NCE) of 25%. DIA scans covered a range of 145–1450 m/z with 3 Th isolation windows. Each DIA window was scanned for 3 ms, and the AGC target was set to 800%.

Data analysis

Thermo .raw data files were analysed using *Spectronaut* (v19.2.240905.62635, Biognosys AG[94]) with BGS Factory Settings for directDIA mode against the curated UniProt mouse (UP000000589, 17,227 entries; downloaded January 2025) and *Candida albicans* (UP000000559, 6036 entries; downloaded January 2026) proteomes for protein inference at a 1% FDR. Fixed modifications were set as carbamidomethylation of C, and variable modifications were oxidation of M and N-terminal acetylation. Trypsin was selected as the enzyme, with a missed cleavage allowance of 2. A protein-level report was exported, and *DIA-Analyst* (https://analyst-suites.org/apps/dia-analyst/) was used to perform Perseus-type imputation of missing values. The resulting protein imputed matrix was downloaded for subsequent bioinformatic analysis in *RStudio* (version 2025.05.0 Build 496; R version 4.5.0), filtered to retain only mouse proteins and raw intensity values were $\log_2$-transformed. Differential protein abundance analysis was performed using the *limma* package as described above for mouse transcriptomics data.

Metabolomics analysis of kidney interstitial fluid

Fluid collection and processing

Right kidneys were removed immediately after cull by cervical dislocation and decapitation, and capsules were carefully removed without damaging the underlying kidney tissues. Kidneys were briefly washed in ice-cold saline, blotted dry on Whatman paper, added into the top compartment of Spin-X®

centrifuge tube filters with a 0.45 µm cellulose acetate membrane (Corning) and immediately centrifuged at 8,000×*g* and 4°C for 10 min. The recovered kidney interstitial fluid was transferred to safe-lock microcentrifuge tubes (Eppendorf), snap-frozen in liquid nitrogen and kept at -80°C until extraction and analysis. Kidney tissue remained largely intact, as confirmed by histology.

Per µl of sample, 20 µl of extraction solvent (1:1 acetonitrile:methanol) with a mixture of 17 ^{13}C,^{15}N-labelled amino acids as internal standards (MSK-A2-1.2, Cambridge Isotope Laboratories) were added. Samples were incubated on a Thermomixer (Eppendorf) for 10 min at 4°C and 2000 rpm prior to centrifugation at 22,000×*g* for 15 min at 4°C. Supernatants were transferred to LC-MS vials for analysis. 10 µl of a Pooled Quality Control (PQC) sample was prepared from samples with ≥ 2 µl of fluid (*n* = 23).

Liquid chromatography-mass spectrometry

Sample extracts were randomised for LC-MS, with PQCs injected every 6th sample and blank injections before and after the run to assess instrument performance. Sample extracts were resolved for untargeted polar metabolomics by hydrophilic interaction liquid chromatography (HILIC) coupled to high-resolution mass spectrometry (MS). Chromatographic separation was achieved with a polymeric HILIC column (iHILIC®-(P) Classic, HILIC Column, PEEK,150x4.6mm, 5µm, 200Å) at 25°C with a gradient elution of 20 mM ammonium carbonate (A) and acetonitrile (B) (linear gradient time-%B as follows: 0 min-80%, 15 min-50%, 18 min-5%, 21 min-5%, 24 min-80%, 32 min-80%) on a Vanquish Horizon UHPLC (Thermo Fisher Scientific). The flow rate was maintained at 500 µl/min. Samples were kept at 6°C in the autosampler, and 10 µl was injected for analysis. Mass spectrometry was performed on an Exploris 480 Orbitrap (Thermo Fisher Scientific) in MS1 polarity-switching mode. The instrument was operated at 120,000 resolution with the following conditions: Electrospray ionisation voltage: 3.5 kV in positive and −2.5 kV in negative mode, capillary temperature: 325°C; sheath gas: 60; Aux gas: 15; spare gas: 2; vaporiser temperature: 350°C.

To support metabolite identification, a standard library of ~ 400 metabolites was analysed at the time of the experiment and accurate retention times for each standard were used for level 1 identification of present metabolites[95]. This standard library also formed the basis of a retention time prediction model used to provide putative identification of metabolites not contained within the standard library[96].

Data analysis

Acquired data were processed for untargeted metabolomics using open-source software IDEOM, which initially used *msConvert* (*ProteoWizard*)[97] to convert raw LC-MS files to *mzXML* format and *XCMS* to pick peaks to convert to *.peakML* files[98]. *Mzmatch* was subsequently used for sample alignment and filtering[99]. Retention times for the standard library were extracted using the targeted peak detection module in MZmine (version 2.53[100]). Samples were processed using IDEOM (version 25[98]) with the default parameters. Mean mass error for identification was less than 1 ppm, so no mass recalibration was performed. Identified peaks were checked in IDEOM, and features with obviously poor chromatography (low intensity, very early/late retention time, no peak) or only present in PQC or fewer

than 10 samples were moved to the Rejected sheet. Subsequent analysis was performed in *RStudio* (version 2025.05.0 Build 496; R version 4.5.0). Identified untargeted metabolomics raw intensity values were median-normalised and $\log_2$-transformed, with missing value imputation set to one-fifth of the lowest detected intensity value for each metabolite. Downstream analyses were restricted to 164 endogenous metabolites validated by comparison to the standard library. The full data set is explorable through the *CanDi* app (https://github.com/hstoelting/CanDi). Differential metabolite abundance analysis was performed using the *limma* package as described above for mouse transcriptomics and proteomics data.

Statistical analysis and data visualisation

Unless stated otherwise, all data analysis and visualisation were conducted in *RStudio* (version 2025.05.0 Build 496; R version 4.5.0). The *stats* (version 4.5.0) and *rstatix* (version 0.7.2) packages were used for statistical analyses. Details of sample sizes, the number of technical replicates and independent repeats, and the types of statistical tests performed are provided in the figure legends. Unless stated otherwise, continuous variables comparing two groups were evaluated by calculating exact *P* values using a two-sided Mann-Whitney *U* test for unpaired or a Wilcoxon signed-rank test for paired data, respectively, with *P* values below 0.05 being considered statistically significant. For three or more groups, a Kruskal-Wallis test followed by a Dunn's post-hoc test with Holm's correction for multiple comparisons was used. To evaluate simultaneous effects of T2D phenotype and time to humane endpoint on gene expression, $\log_2$-transformed relative expression levels were analysed using a two-way additive Analysis of Variance (ANOVA). The relationship between fungal burden assays was determined by calculating Pearson's correlation coefficients between $\log_{10}$-transformed CFU or fungal housekeeping gene expression values. Differences in occurrence of categorical variables between two experimental groups were determined using Pearson's chi-square test. Differences in survival (time to humane endpoint) distributions between phenotypes were estimated using the log-rank (Mantel-Cox) test via the *survival* package (3.8-6). Significance levels are reported in figure panels as follows: **p* < 0.05, ***p* < 0.01, ****p* < 0.001, and *****p* < 0.0001. All statistical testing was two-tailed. Graphs were created using *ggplot2* (version 4.0.2) and *eulerr* (7.0.4). Unless stated otherwise, data are shown as box plots showing the median, interquartile range (box bounds) and min-to-max range (whiskers). Individual data points are overlaid where applicable, with paired observations linked by lines. Schematics and graphical illustrations were created using Adobe Illustrator (version 30.2.1).

To facilitate interactive exploration of the integrated multi-omics data sets (metabolomics, transcriptomics and proteomics), the custom web application *CanDi* (Candida in Diabetes) was developed using the *shiny* (version 1.13.0) and *bslib* (version 0.10.0) packages. The *CanDi* application is publicly accessible at https://github.com/hstoelting/CanDi.

Declarations

ACKNOWLEDGMENTS

We acknowledge the support and technical assistance of the Monash University Animal Research Platform, Genomics and Bioinformatics Platform, Histology Platform, and Proteomics and Metabolomics Platform and thank Andrew Perry for his assistance with the Shiny App. This study utilised infrastructure enabled by Bioplatforms Australia (BPA) and the National Collaborative Research Infrastructure Strategy (NCRIS), located at the Monash Proteomics and Metabolomics Platform. This research was supported by Monash eResearch capabilities, including M3, Research Data Storage and Nectar Research Cloud.

This research was supported by a National Health and Medical Research Council of Australia (NHMRC) Ideas grant 2019765 (to A.T. and A.J.R.), Investigator Grant 2033452 (to A.T.), and a Monash University Faculty of Medicine, Nursing and Health Sciences Platform Access Grant (to H.S. and A.M.).

AUTHOR CONTRIBUTIONS

Conceptualization: H.S., A.J.R., A.T.

Methodology: H.S., A.M., A.J.R.

Investigation: H.S., A.G., H.W., Y.W., D.H.M., K.J.J., C.K.B., K.O'S., P.M.R.

Funding acquisition: H.S., A.M., A.J.R., A.T.

Resources: K.O'S., A.J.R., A.T

Visualisation: H.S.

Supervision: R.B.S., A.J.R., A.T.

Writing – original draft: H.S., A.J.R., A.T.

Writing – review & editing: H.S., K.J.J., R.B.S., A.J.R., A.T.

DECLARATION OF INTERESTS

P.M.R. & A.J.R. have received funding from Boehringer-Ingelheim, a pharmaceutical company, for an unrelated project. The other authors declare no competing interests.

DECLARATION OF GENERATIVE AI AND AI-ASSISTED TECHNOLOGIES in the writing process

No generative AI or AI-assisted technologies were used in the writing, drafting, or editing of the manuscript text, nor in the generation of figures. The author used OpenAI ChatGPT and Google Gemini as an auxiliary tool to assist in scripting and developing the code for the Interactive Shiny application. All code was manually audited, debugged, and validated, and the authors take full responsibility for the content of the publication.

DATA AVAILABILITY

Data generated in this study are provided in the manuscript and supplementary information. The mass spectrometry proteomics data have been deposited to the ProteomeXchange Consortium via the PRIDE[93] partner repository with the dataset identifier PXD083872. Raw and processed RNA-seq data have been deposited in the NCBI Gene Expression Omnibus under the accession number GSE346796. The interactive *CanDi* Shiny application, along with all underlying code, is available in the GitHub repository at https://github.com/hstoelting/CanDi.

References

1. Weerasinghe, H., Stolting, H., Rose, A.J., and Traven, A. (2024). Metabolic homeostasis in fungal infections from the perspective of pathogens, immune cells, and whole-body systems. Microbiol Mol Biol Rev *88*, e0017122. 10.1128/mmbr.00171-22.
2. Rosenberg, G., Riquelme, S., Prince, A., and Avraham, R. (2022). Immunometabolic crosstalk during bacterial infection. Nat Microbiol *7*, 497–507. 10.1038/s41564-022-01080-5.
3. Brown, A.J., Brown, G.D., Netea, M.G., and Gow, N.A. (2014). Metabolism impacts upon Candida immunogenicity and pathogenicity at multiple levels. Trends Microbiol *22*, 614–622. 10.1016/j.tim.2014.07.001.
4. Troha, K., and Ayres, J.S. (2020). Metabolic Adaptations to Infections at the Organismal Level. Trends Immunol *41*, 113–125. 10.1016/j.it.2019.12.001.
5. Denning, D.W. (2024). Global incidence and mortality of severe fungal disease. Lancet Infect Dis *24*, e428–e438. 10.1016/S1473-3099(23)00692-8.
6. Askew, C., Sellam, A., Epp, E., Hogues, H., Mullick, A., Nantel, A., and Whiteway, M. (2009). Transcriptional regulation of carbohydrate metabolism in the human pathogen Candida albicans. PLoS Pathog *5*, e1000612. 10.1371/journal.ppat.1000612.
7. Tucey, T.M., Verma, J., Harrison, P.F., Snelgrove, S.L., Lo, T.L., Scherer, A.K., Barugahare, A.A., Powell, D.R., Wheeler, R.T., Hickey, M.J., et al. (2018). Glucose Homeostasis Is Important for Immune Cell Viability during Candida Challenge and Host Survival of Systemic Fungal Infection. Cell Metab *27*, 988–1006 e1007. 10.1016/j.cmet.2018.03.019.
8. Barelle, C.J., Priest, C.L., Maccallum, D.M., Gow, N.A., Odds, F.C., and Brown, A.J. (2006). Niche-specific regulation of central metabolic pathways in a fungal pathogen. Cell Microbiol *8*, 961–971. 10.1111/j.1462-5822.2005.00676.x.
9. Li, D.D., Jawale, C.V., Zhou, C., Lin, L., Trevejo-Nunez, G.J., Rahman, S.A., Mullet, S.J., Das, J., Wendell, S.G., Delgoffe, G.M., et al. (2022). Fungal sensing enhances neutrophil metabolic fitness by regulating antifungal Glut1 activity. Cell Host Microbe *30*, 530–544 e536. 10.1016/j.chom.2022.02.017.
10. Jawale, C.V., Ramani, K., Li, D.D., Coleman, B.M., Oberoi, R.S., Kupul, S., Lin, L., Desai, J.V., Delgoffe, G.M., Lionakis, M.S., et al. (2020). Restoring glucose uptake rescues neutrophil dysfunction and

protects against systemic fungal infection in mouse models of kidney disease. Sci Transl Med *12*. 10.1126/scitranslmed.aay5691.

11. Dominguez-Andres, J., Arts, R.J.W., Ter Horst, R., Gresnigt, M.S., Smeekens, S.P., Ratter, J.M., Lachmandas, E., Boutens, L., van de Veerdonk, F.L., Joosten, L.A.B., et al. (2017). Rewiring monocyte glucose metabolism via C-type lectin signaling protects against disseminated candidiasis. PLoS Pathog *13*, e1006632. 10.1371/journal.ppat.1006632.
12. Weerasinghe, H., Tulyaprawat, O., Stolting, H., Sonnberger, J., Mobbs, B., Nickson, J., Lange, T., van Denderen, B., Lo, T.L., Schille, T.B., et al. (2026). Infection-induced glucose starvation triggers NINJ1-dependent macrophage lysis and Candida escape. Nat Commun *17*. 10.1038/s41467-026-74195-6.
13. Cheng, S.C., Scicluna, B.P., Arts, R.J., Gresnigt, M.S., Lachmandas, E., Giamarellos-Bourboulis, E.J., Kox, M., Manjeri, G.R., Wagenaars, J.A., Cremer, O.L., et al. (2016). Broad defects in the energy metabolism of leukocytes underlie immunoparalysis in sepsis. Nat Immunol *17*, 406–413. 10.1038/ni.3398.
14. Rodrigues, C.F., Rodrigues, M.E., and Henriques, M. (2019). Candida sp. Infections in Patients with Diabetes Mellitus. J Clin Med *8*. 10.3390/jcm8010076.
15. Cornely, O.A., Sprute, R., Bassetti, M., Chen, S.C., Groll, A.H., Kurzai, O., Lass-Florl, C., Ostrosky-Zeichner, L., Rautemaa-Richardson, R., Revathi, G., et al. (2025). Global guideline for the diagnosis and management of candidiasis: an initiative of the ECMM in cooperation with ISHAM and ASM. Lancet Infect Dis *25*, e280–e293. 10.1016/S1473-3099(24)00749-7.
16. Araujo, J.M., de Almeida Junior, J.N., Magri, M.M.C., Costa, S.F., and Guimaraes, T. (2024). Epidemiological Assessment and Risk Factors for Mortality of Bloodstream Infections by Candida sp. and the Impact of the COVID-19 Pandemic Era. J Fungi (Basel) *10*. 10.3390/jof10040268.
17. Jenkins, E.N., Gold, J.A.W., Benedict, K., Lockhart, S.R., Berkow, E.L., Dixon, T., Shack, S.L., Witt, L.S., Harrison, L.H., Seopaul, S., et al. (2025). Population-Based Active Surveillance for Culture-Confirmed Candidemia - 10 Sites, United States, 2017-2021. MMWR Surveill Summ *74*, 1–15. 10.15585/mmwr.ss7404a1.
18. Genitsaridi, I., Salpea, P., Salim, A., Sajjadi, S.F., Tomic, D., James, S., Thirunavukkarasu, S., Issaka, A., Chen, L., Basit, A., et al. (2026). 11th edition of the IDF Diabetes Atlas: global, regional, and national diabetes prevalence estimates for 2024 and projections for 2050. Lancet Diabetes Endocrinol *14*, 149–156. 10.1016/S2213-8587(25)00299-2.
19. Collaboration, N.C.D.R.F. (2024). Worldwide trends in diabetes prevalence and treatment from 1990 to 2022: a pooled analysis of 1108 population-representative studies with 141 million participants. Lancet *404*, 2077–2093. 10.1016/S0140-6736(24)02317-1.
20. Disease, G.B.D., Injury, and Risk Factor, C. (2025). Burden of 375 diseases and injuries, risk-attributable burden of 88 risk factors, and healthy life expectancy in 204 countries and territories, including 660 subnational locations, 1990-2023: a systematic analysis for the Global Burden of Disease Study 2023. Lancet *406*, 1873–1922. 10.1016/S0140-6736(25)01637-X.

21. Mlynarska, E., Czarnik, W., Dzieza, N., Jedraszak, W., Majchrowicz, G., Prusinowski, F., Stabrawa, M., Rysz, J., and Franczyk, B. (2025). Type 2 Diabetes Mellitus: New Pathogenetic Mechanisms, Treatment and the Most Important Complications. Int J Mol Sci *26*. 10.3390/ijms26031094.
22. World Health, O. (2024). Diabetes: coverage of treatment with glucose-lowering medication (age-standardized).
23. Mencacci, A., Romani, L., Mosci, P., Cenci, E., Tonnetti, L., Vecchiarelli, A., and Bistoni, F. (1993). Low-dose streptozotocin-induced diabetes in mice. II. Susceptibility to Candida albicans infection correlates with the induction of a biased Th2-like antifungal response. Cell Immunol *150*, 36–44. 10.1006/cimm.1993.1176.
24. Mosci, P., Vecchiarelli, A., Cenci, E., Puliti, M., and Bistoni, F. (1993). Low-dose streptozotocin-induced diabetes in mice. I. Course of Candida albicans infection. Cell Immunol *150*, 27–35. 10.1006/cimm.1993.1175.
25. Plotkin, B.J., Paulson, D., Chelich, A., Jurak, D., Cole, J., Kasimos, J., Burdick, J.R., and Casteel, N. (1996). Immune responsiveness in a rat model for type II diabetes (Zucker rat, fa/fa): susceptibility to Candida albicans infection and leucocyte function. J Med Microbiol *44*, 277–283. 10.1099/00222615-44-4-277.
26. Fraga-Silva, T.F., Venturini, J., and de Arruda, M.S. (2013). Trafficking of phagocytic peritoneal cells in hypoinsulinemic-hyperglycemic mice with systemic candidiasis. BMC Infect Dis *13*, 147. 10.1186/1471-2334-13-147.
27. Venturini, J., Fraga-Silva, T.F., Marchetti, C.M., Mimura, L.A., Conti, B.J., Golim Mde, A., Mendes, R.P., and de Arruda, M.S. (2016). Imbalanced Macrophage and Dendritic Cell Activations in Response to Candida albicans in a Murine Model of Diabetes Mellitus. Immunol Invest *45*, 420–438. 10.3109/08820139.2016.1162798.
28. Harpf, V., Kenno, S., Rambach, G., Fleischer, V., Parth, N., Weichenberger, C.X., Garred, P., Huber, S., Lass-Florl, C., Speth, C., and Wurzner, R. (2022). Influence of Glucose on Candida albicans and the Relevance of the Complement FH-Binding Molecule Hgt1 in a Murine Model of Candidiasis. Antibiotics (Basel) *11*. 10.3390/antibiotics11020257.
29. Khan, M.A., Aldebasi, Y.H., Alsuhaibani, S.A., AlSahli, M.A., Alzohairy, M.A., Khan, A., and Younus, H. (2018). Therapeutic potential of thymoquinone liposomes against the systemic infection of Candida albicans in diabetic mice. PLoS One *13*, e0208951. 10.1371/journal.pone.0208951.
30. Reyna, D.E., Davis, E., Salina, A.C.G., Blackman, A., Martinez-Barricarte, R., Doran, A., and Serezani, C.H. (2026). Hyperglycemia promotes maladaptive Dectin-1 signaling and impairs skin antifungal host defense. bioRxiv. 10.64898/2026.02.11.705431.
31. Gupta, K.D., Quintanilla, D., Youssef, E.G., Gupta, K., Ibrahim, A.S., and Singh, S. (2026). Diabetes and Immunosuppression Drive Distinct Patterns of Candidozyma auris Skin Colonization and Dissemination in Mice. bioRxiv. 10.64898/2026.05.24.727467.
32. Li, H., Tang, D., Chen, J., Hu, Y., Cai, X., and Zhang, P. (2021). The Clinical Value of GDF15 and Its Prospective Mechanism in Sepsis. Front Immunol *12*, 710977. 10.3389/fimmu.2021.710977.

33. Luan, H.H., Wang, A., Hilliard, B.K., Carvalho, F., Rosen, C.E., Ahasic, A.M., Herzog, E.L., Kang, I., Pisani, M.A., Yu, S., et al. (2019). GDF15 Is an Inflammation-Induced Central Mediator of Tissue Tolerance. Cell *178*, 1231–1244 e1211. 10.1016/j.cell.2019.07.033.

34. Santos, I., Colaco, H.G., Neves-Costa, A., Seixas, E., Velho, T.R., Pedroso, D., Barros, A., Martins, R., Carvalho, N., Payen, D., et al. (2020). CXCL5-mediated recruitment of neutrophils into the peritoneal cavity of Gdf15-deficient mice protects against abdominal sepsis. Proc Natl Acad Sci U S A *117*, 12281–12287. 10.1073/pnas.1918508117.

35. Moyes, D.L., Wilson, D., Richardson, J.P., Mogavero, S., Tang, S.X., Wernecke, J., Hofs, S., Gratacap, R.L., Robbins, J., Runglall, M., et al. (2016). Candidalysin is a fungal peptide toxin critical for mucosal infection. Nature *532*, 64–68. 10.1038/nature17625.

36. Mirhashemi, F., Scherneck, S., Kluth, O., Kaiser, D., Vogel, H., Kluge, R., Schurmann, A., Neschen, S., and Joost, H.G. (2011). Diet dependence of diabetes in the New Zealand Obese (NZO) mouse: total fat, but not fat quality or sucrose accelerates and aggravates diabetes. Exp Clin Endocrinol Diabetes *119*, 167–171. 10.1055/s-0030-1263127.

37. Lionakis, M.S., Swamydas, M., Fischer, B.G., Plantinga, T.S., Johnson, M.D., Jaeger, M., Green, N.M., Masedunskas, A., Weigert, R., Mikelis, C., et al. (2013). CX3CR1-dependent renal macrophage survival promotes Candida control and host survival. J Clin Invest *123*, 5035–5051. 10.1172/JCI71307.

38. Xu, S., and Shinohara, M.L. (2017). Tissue-Resident Macrophages in Fungal Infections. Front Immunol *8*, 1798. 10.3389/fimmu.2017.01798.

39. Desai, J.V., and Lionakis, M.S. (2018). The role of neutrophils in host defense against invasive fungal infections. Curr Clin Microbiol Rep *5*, 181–189. 10.1007/s40588-018-0098-6.

40. Vonk, A.G., Netea, M.G., van Krieken, J.H., Iwakura, Y., van der Meer, J.W., and Kullberg, B.J. (2006). Endogenous interleukin (IL)-1 alpha and IL-1 beta are crucial for host defense against disseminated candidiasis. J Infect Dis *193*, 1419–1426. 10.1086/503363.

41. Gozalbo, D., Maneu, V., and Gil, M.L. (2014). Role of IFN-gamma in immune responses to Candida albicans infections. Front Biosci (Landmark Ed) *19*, 1279–1290. 10.2741/4281.

42. Prasad, R.B., and Groop, L. (2019). Precision medicine in type 2 diabetes. J Intern Med *285*, 40–48. 10.1111/joim.12859.

43. Kleinert, M., Clemmensen, C., Hofmann, S.M., Moore, M.C., Renner, S., Woods, S.C., Huypens, P., Beckers, J., de Angelis, M.H., Schurmann, A., et al. (2018). Animal models of obesity and diabetes mellitus. Nat Rev Endocrinol *14*, 140–162. 10.1038/nrendo.2017.161.

44. Gray, V., Chen, W., Tan, R.J.Y., Teo, J.M.N., Huang, Z., Fong, C.H., Law, T.W.H., Ye, Z.W., Yuan, S., Bao, X., et al. (2024). Hyperglycemia-triggered lipid peroxidation destabilizes STAT4 and impairs anti-viral Th1 responses in type 2 diabetes. Cell Metab *36*, 2511–2527 e2517. 10.1016/j.cmet.2024.10.004.

45. Nobs, S.P., Kolodziejczyk, A.A., Adler, L., Horesh, N., Botscharnikow, C., Herzog, E., Mohapatra, G., Hejndorf, S., Hodgetts, R.J., Spivak, I., et al. (2023). Lung dendritic-cell metabolism underlies susceptibility to viral infection in diabetes. Nature *624*, 645–652. 10.1038/s41586-023-06803-0.

46. Javid, A., Zlotnikov, N., Petrosova, H., Tang, T.T., Zhang, Y., Bansal, A.K., Ebady, R., Parikh, M., Ahmed, M., Sun, C., et al. (2016). Hyperglycemia Impairs Neutrophil-Mediated Bacterial Clearance in Mice Infected with the Lyme Disease Pathogen. PLoS One *11*, e0158019. 10.1371/journal.pone.0158019.
47. Bhatwa, A., Lau, T.C., McPhee, J.B., Anhe, F.F., Anhe, G.F., Fang, H., Barra, N.G., Li, Y., Duggan, B.M., Chan, D.Y., et al. (2025). Hyperglycemia worsens gut bacterial infection through intestinal Wnt, but independent of endotoxemia or obesity. Am J Physiol Endocrinol Metab *329*, E441–E454. 10.1152/ajpendo.00251.2025.
48. Seo, K.S., Park, N., Rutter, J.K., Park, Y., Baker, C.L., Thornton, J.A., and Park, J.Y. (2021). Role of Glucose-6-Phosphate in Metabolic Adaptation of Staphylococcus aureus in Diabetes. Microbiol Spectr *9*, e0085721. 10.1128/Spectrum.00857-21.
49. Astrand, A., Wingren, C., Benjamin, A., Tregoning, J.S., Garnett, J.P., Groves, H., Gill, S., Orogo-Wenn, M., Lundqvist, A.J., Walters, D., et al. (2017). Dapagliflozin-lowered blood glucose reduces respiratory Pseudomonas aeruginosa infection in diabetic mice. Br J Pharmacol *174*, 836–847. 10.1111/bph.13741.
50. Fiocca Vernengo, F., Rowekamp, I., Boillot, L., Caesar, S., Dorner, P.J., Tarnowski, B., Gutbier, B., Nouailles, G., Fatykhova, D., Hellwig, K., et al. (2025). Diabetes impairs IFNgamma-dependent antibacterial defense in the lungs. Mucosal Immunol *18*, 431–440. 10.1016/j.mucimm.2024.12.015.
51. Barber, K.E., Wagner, J.L., Miller, J.M., Lewis, E.A., and Stover, K.R. (2020). Impact of Obesity in Patients with Candida Bloodstream Infections: A Retrospective Cohort Study. Infect Dis Ther *9*, 175–183. 10.1007/s40121-020-00285-7.
52. Vinayagamoorthy, K., Pentapati, K.C., and Prakash, H. (2022). Prevalence, risk factors, treatment and outcome of multidrug resistance Candida auris infections in Coronavirus disease (COVID-19) patients: A systematic review. Mycoses *65*, 613–624. 10.1111/myc.13447.
53. Roden, M., and Shulman, G.I. (2019). The integrative biology of type 2 diabetes. Nature *576*, 51–60. 10.1038/s41586-019-1797-8.
54. Petersen, M.C., and Shulman, G.I. (2018). Mechanisms of Insulin Action and Insulin Resistance. Physiol Rev *98*, 2133–2223. 10.1152/physrev.00063.2017.
55. Kaposzta, R., Tree, P., Marodi, L., and Gordon, S. (1998). Characteristics of invasive candidiasis in gamma interferon- and interleukin-4-deficient mice: role of macrophages in host defense against Candida albicans. Infect Immun *66*, 1708–1717. 10.1128/IAI.66.4.1708-1717.1998.
56. Charpak-Amikam, Y., Kournos, M., Kotzur, R., Isaacson, B., Bagad Brenner, T., Gomez-Cesar, E., Abou-Kandil, A., Ben-Ami, R., Korem, M., Guerra, N., et al. (2024). The activating receptor NKG2D is an anti-fungal pattern recognition receptor. Nat Commun *15*, 8664. 10.1038/s41467-024-52913-2.
57. Schmidt, S., Tramsen, L., and Lehrnbecher, T. (2017). Natural Killer Cells in Antifungal Immunity. Front Immunol *8*, 1623. 10.3389/fimmu.2017.01623.
58. de Souza Ferreira, C., Pennacchi, P.C., Araujo, T.H., Taniwaki, N.N., de Araujo Paula, F.B., da Silveira Duarte, S.M., and Rodrigues, M.R. (2016). Aminoguanidine treatment increased NOX2 response in

diabetic rats: Improved phagocytosis and killing of Candida albicans by neutrophils. Eur J Pharmacol *772*, 83–91. 10.1016/j.ejphar.2015.12.044.

59. Wilson, R.M., and Reeves, W.G. (1986). Neutrophil phagocytosis and killing in insulin-dependent diabetes. Clin Exp Immunol *63*, 478–484.
60. Wong, S.L., Demers, M., Martinod, K., Gallant, M., Wang, Y., Goldfine, A.B., Kahn, C.R., and Wagner, D.D. (2015). Diabetes primes neutrophils to undergo NETosis, which impairs wound healing. Nat Med *21*, 815–819. 10.1038/nm.3887.
61. Xiao, M., Xu, Z., Zhu, X., Chen, J., Wang, R., Wang, Y., Gao, X., Luan, S., and Pu, X. (2025). Immunological profiling in type 2 diabetes mellitus and type 2 diabetic kidney disease: insights from single-cell LacNAc sequencing. Front Endocrinol (Lausanne) *16*, 1550925. 10.3389/fendo.2025.1550925.
62. Joshi, M.B., Ahamed, R., Hegde, M., Nair, A.S., Ramachandra, L., and Satyamoorthy, K. (2020). Glucose induces metabolic reprogramming in neutrophils during type 2 diabetes to form constitutive extracellular traps and decreased responsiveness to lipopolysaccharides. Biochim Biophys Acta Mol Basis Dis *1866*, 165940. 10.1016/j.bbadis.2020.165940.
63. Fajgenbaum, D.C., and June, C.H. (2020). Cytokine Storm. N Engl J Med *383*, 2255–2273. 10.1056/NEJMra2026131.
64. Fan, J.B., Li, Q.Y., Feng, X.F., Huang, S.Y., Wang, R., Liao, F.Y., Liu, D., Liu, W.Y., Sun, J.H., Zhang, H.C., et al. (2026). The "cytokine storm" in infection and sepsis: win the battle but lose the war. Mil Med Res *12*, 95. 10.1186/s40779-025-00678-0.
65. Zhu, L., She, Z.G., Cheng, X., Qin, J.J., Zhang, X.J., Cai, J., Lei, F., Wang, H., Xie, J., Wang, W., et al. (2020). Association of Blood Glucose Control and Outcomes in Patients with COVID-19 and Pre-existing Type 2 Diabetes. Cell Metab *31*, 1068–1077 e1063. 10.1016/j.cmet.2020.04.021.
66. Guo, W., Li, M., Dong, Y., Zhou, H., Zhang, Z., Tian, C., Qin, R., Wang, H., Shen, Y., Du, K., et al. (2020). Diabetes is a risk factor for the progression and prognosis of COVID-19. Diabetes Metab Res Rev *36*, e3319. 10.1002/dmrr.3319.
67. Apicella, M., Campopiano, M.C., Mantuano, M., Mazoni, L., Coppelli, A., and Del Prato, S. (2020). COVID-19 in people with diabetes: understanding the reasons for worse outcomes. Lancet Diabetes Endocrinol *8*, 782–792. 10.1016/S2213-8587(20)30238-2.
68. Li, S., Yang, L., Feng, X., Peng, X., Zhang, J., Liu, M., and Li, K. (2026). Clinical characteristics and risk factors of mortality in patients with candidemia: a four-year retrospective study. Eur J Clin Microbiol Infect Dis *45*, 383–393. 10.1007/s10096-025-05324-0.
69. Kartika, R., Purnamasari, D., Pradipta, S., Larasati, R.A., and Wibowo, H. (2020). Impact of Low Interferon-gamma and IL-10 Levels on TNF-alpha and IL-6 Production by PHA-Induced PBMCs in Type 2 Diabetes Mellitus. J Inflamm Res *13*, 187–193. 10.2147/JIR.S245064.
70. Tan, K.S., Lee, K.O., Low, K.C., Gamage, A.M., Liu, Y., Tan, G.Y., Koh, H.Q., Alonso, S., and Gan, Y.H. (2012). Glutathione deficiency in type 2 diabetes impairs cytokine responses and control of intracellular bacteria. J Clin Invest *122*, 2289–2300. 10.1172/JCI57817.

71. Bosek, I., Kuczerowski, R., Milek, T., Sulich, A., Kaleta, B., Kniotek, M., and Piatkiewicz, P. (2015). Evaluation of Interferon-Gamma in Patients with Type 2 Diabetes and Colorectal Cancer. Journal of Diabetes & Metabolism *07*. 10.4172/2155-6156.1000639.
72. Tsiavou, A., Hatziagelaki, E., Chaidaroglou, A., Koniavitou, K., Degiannis, D., and Raptis, S.A. (2005). Correlation between intracellular interferon-gamma (IFN-gamma) production by CD4+ and CD8+ lymphocytes and IFN-gamma gene polymorphism in patients with type 2 diabetes mellitus and latent autoimmune diabetes of adults (LADA). Cytokine *31*, 135–141. 10.1016/j.cyto.2005.02.011.
73. Marissa, N., Marlinda, M., Maulidar, M., Wilya, V., Ramadhan, N., Hadifah, Z., and Nur, A. (2021). Interferon gamma concentration in diabetes mellitus and dyslipidemia patient. Health Science Journal of Indonesia *12*, 74–80. 10.22435/hsji.v12i2.4290.
74. Liu, S., Jayasinghe, T., Kaminska, D., Xu, X., Ren, X., Jiao, Y., Kong, Y., Li, X., Li, K., Antoniou, A.N., et al. (2025). Augmented MHC Class I on Professional Antigen-Presenting Cells and Enhanced Cytokine Production by CD8(+) T Cells in Type 2 Diabetes Mellitus. Eur J Immunol *55*, e70109. 10.1002/eji.70109.
75. Bahgat, M.M., and Ibrahim, D.R. (2020). Proinflammatory cytokine polarization in type 2 diabetes. Cent Eur J Immunol *45*, 170–175. 10.5114/ceji.2020.97904.
76. Zhao, J., and Fang, Z. (2024). Single-cell RNA sequencing reveals the dysfunctional characteristics of PBMCs in patients with type 2 diabetes mellitus. Front Immunol *15*, 1501660. 10.3389/fimmu.2024.1501660.
77. Omodaka, S., Kato, Y., Sato, Y., Falcone-Juengert, J., Zhang, H., Kanoke, A., Eckalbar, W.L., Endo, H., Hsieh, C.L., Aran, D., and Liu, J. (2024). Defective interferon signaling in the circulating monocytes of type 2 diabetic mice. bioRxiv. 10.1101/2024.06.03.597050.
78. Yoon Kim, D., and Kwon Lee, J. (2022). Type 1 and 2 diabetes are associated with reduced natural killer cell cytotoxicity. Cell Immunol *379*, 104578. 10.1016/j.cellimm.2022.104578.
79. Berrou, J., Fougeray, S., Venot, M., Chardiny, V., Gautier, J.F., Dulphy, N., Toubert, A., and Peraldi, M.N. (2013). Natural killer cell function, an important target for infection and tumor protection, is impaired in type 2 diabetes. PLoS One *8*, e62418. 10.1371/journal.pone.0062418.
80. Kim, J.H., Park, K., Lee, S.B., Kang, S., Park, J.S., Ahn, C.W., and Nam, J.S. (2019). Relationship between natural killer cell activity and glucose control in patients with type 2 diabetes and prediabetes. J Diabetes Investig *10*, 1223–1228. 10.1111/jdi.13002.
81. Voigt, J., Hunniger, K., Bouzani, M., Jacobsen, I.D., Barz, D., Hube, B., Loffler, J., and Kurzai, O. (2014). Human natural killer cells acting as phagocytes against Candida albicans and mounting an inflammatory response that modulates neutrophil antifungal activity. J Infect Dis *209*, 616–626. 10.1093/infdis/jit574.
82. Li, S.S., Ogbomo, H., Mansour, M.K., Xiang, R.F., Szabo, L., Munro, F., Mukherjee, P., Mariuzza, R.A., Amrein, M., Vyas, J.M., et al. (2018). Identification of the fungal ligand triggering cytotoxic PRR-mediated NK cell killing of Cryptococcus and Candida. Nat Commun *9*, 751. 10.1038/s41467-018-03014-4.

83. Spellberg, B., Ibrahim, A.S., Edwards, J.E., Jr., and Filler, S.G. (2005). Mice with disseminated candidiasis die of progressive sepsis. J Infect Dis *192*, 336–343. 10.1086/430952.

84. Cruz, M., Maldonado-Bernal, C., Mondragon-Gonzalez, R., Sanchez-Barrera, R., Wacher, N.H., Carvajal-Sandoval, G., and Kumate, J. (2008). Glycine treatment decreases proinflammatory cytokines and increases interferon-gamma in patients with type 2 diabetes. J Endocrinol Invest *31*, 694–699. 10.1007/BF03346417.

85. Lionakis, M.S. (2014). New insights into innate immune control of systemic candidiasis. Med Mycol *52*, 555–564. 10.1093/mmy/myu029.

86. Sprague, J.L., Kasper, L., and Hube, B. (2022). From intestinal colonization to systemic infections: Candida albicans translocation and dissemination. Gut Microbes *14*, 2154548. 10.1080/19490976.2022.2154548.

87. Bankhead, P., Loughrey, M.B., Fernandez, J.A., Dombrowski, Y., McArt, D.G., Dunne, P.D., McQuaid, S., Gray, R.T., Murray, L.J., Coleman, H.G., et al. (2017). QuPath: Open source software for digital pathology image analysis. Sci Rep *7*, 16878. 10.1038/s41598-017-17204-5.

88. Schindelin, J., Arganda-Carreras, I., Frise, E., Kaynig, V., Longair, M., Pietzsch, T., Preibisch, S., Rueden, C., Saalfeld, S., Schmid, B., et al. (2012). Fiji: an open-source platform for biological-image analysis. Nat Methods *9*, 676–682. 10.1038/nmeth.2019.

89. Ruifrok, A.C., and Johnston, D.A. (2001). Quantification of histochemical staining by color deconvolution. Anal Quant Cytol Histol *23*, 291–299.

90. Amend, S.R., Valkenburg, K.C., and Pienta, K.J. (2016). Murine Hind Limb Long Bone Dissection and Bone Marrow Isolation. J Vis Exp. 10.3791/53936.

91. Stirling, D.R., Swain-Bowden, M.J., Lucas, A.M., Carpenter, A.E., Cimini, B.A., and Goodman, A. (2021). CellProfiler 4: improvements in speed, utility and usability. BMC Bioinformatics *22*, 433. 10.1186/s12859-021-04344-9.

92. Yu, G., Wang, L.G., Han, Y., and He, Q.Y. (2012). clusterProfiler: an R package for comparing biological themes among gene clusters. OMICS *16*, 284–287. 10.1089/omi.2011.0118.

93. Perez-Riverol, Y., Bai, J., Bandla, C., Garcia-Seisdedos, D., Hewapathirana, S., Kamatchinathan, S., Kundu, D.J., Prakash, A., Frericks-Zipper, A., Eisenacher, M., et al. (2022). The PRIDE database resources in 2022: a hub for mass spectrometry-based proteomics evidences. Nucleic Acids Res *50*, D543–D552. 10.1093/nar/gkab1038.

94. Bruderer, R., Bernhardt, O.M., Gandhi, T., Miladinovic, S.M., Cheng, L.Y., Messner, S., Ehrenberger, T., Zanotelli, V., Butscheid, Y., Escher, C., et al. (2015). Extending the limits of quantitative proteome profiling with data-independent acquisition and application to acetaminophen-treated three-dimensional liver microtissues. Mol Cell Proteomics *14*, 1400–1410. 10.1074/mcp.M114.044305.

95. Sumner, L.W., Amberg, A., Barrett, D., Beale, M.H., Beger, R., Daykin, C.A., Fan, T.W., Fiehn, O., Goodacre, R., Griffin, J.L., et al. (2007). Proposed minimum reporting standards for chemical analysis Chemical Analysis Working Group (CAWG) Metabolomics Standards Initiative (MSI). Metabolomics *3*, 211–221. 10.1007/s11306-007-0082-2.

96. Creek, D.J., Jankevics, A., Breitling, R., Watson, D.G., Barrett, M.P., and Burgess, K.E. (2011). Toward global metabolomics analysis with hydrophilic interaction liquid chromatography-mass spectrometry: improved metabolite identification by retention time prediction. Anal Chem *83*, 8703–8710. 10.1021/ac2021823.
97. Chambers, M.C., Maclean, B., Burke, R., Amodei, D., Ruderman, D.L., Neumann, S., Gatto, L., Fischer, B., Pratt, B., Egertson, J., et al. (2012). A cross-platform toolkit for mass spectrometry and proteomics. Nat Biotechnol *30*, 918–920. 10.1038/nbt.2377.
98. Creek, D.J., Jankevics, A., Burgess, K.E., Breitling, R., and Barrett, M.P. (2012). IDEOM: an Excel interface for analysis of LC-MS-based metabolomics data. Bioinformatics *28*, 1048–1049. 10.1093/bioinformatics/bts069.
99. Scheltema, R.A., Jankevics, A., Jansen, R.C., Swertz, M.A., and Breitling, R. (2011). PeakML/mzMatch: a file format, Java library, R library, and tool-chain for mass spectrometry data analysis. Anal Chem *83*, 2786–2793. 10.1021/ac2000994.
100. Pluskal, T., Castillo, S., Villar-Briones, A., and Oresic, M. (2010). MZmine 2: modular framework for processing, visualizing, and analyzing mass spectrometry-based molecular profile data. BMC Bioinformatics *11*, 395. 10.1186/1471-2105-11-395.

Figures

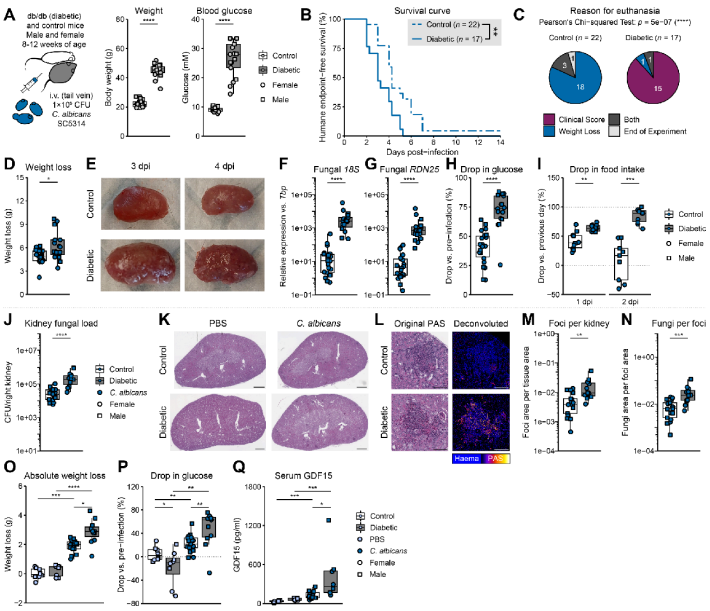


Figure 1. T2D exacerbates disease severity in systemic *C. albicans* infection

(A) 8- to 12-week-old T2D (db/db) or control mice of both sexes were intravenously infected with 1×10^5 CFU *C. albicans*. Graphs show body weight and blood glucose levels prior to infection. Mann-Whitney *U* test.
(B) Kaplan-Meier curve showing time to humane endpoint. Log-rank analysis.
(C) Reasons for euthanasia during survival experiment. Pearson's chi-squared test.
(D) Absolute weight loss during survival experiment. n=17-22 animals per group. Mann-Whitney *U* test.
(E) Photographs of kidneys collected at humane endpoint.
(F and G) Expression of fungal housekeeping genes *18S* (F) and *RDN25* (G) relative to murine housekeeping gene *Tbp* by qPCR in kidneys collected at humane endpoint. n=17-22 animals per group. Mann-Whitney *U* test.
(H) Relative drop in blood glucose compared to pre-infection levels from survival study. n=17-22 animals per group. Mann-Whitney *U* test.
(I) Relative drop in food intake compared to previous day during first two days of survival study. n=10 animals per group. Mann-Whitney *U* test.
(J) Kidney fungal burden in T2D and control mice culled at 24 hours post-infection. n=11-17 animals per group. Mann-Whitney *U* test.
(K) Representative images of PAS staining of kidney sections from T2D or control mice infected with *C. albicans* for 24 hours. Size of scale bar: 1 mm.
(L) Zoomed-in images of original (left) or deconvoluted and pseudo-coloured (right) PAS staining of kidneys from infected T2D and control mice. Colours: blue, haematoxylin; fire scale, PAS. Size of scale bar: 100 µm.
(M and N) Quantification of PAS images. Relative area of inflammatory foci per kidney (M) and PAS$^+$ fungi per foci (N) of infected T2D and control mice at 24 hours post-infection. n=11-17 animals per group. Mann-Whitney *U* test.
(O) Absolute weight loss at 24 hours post-infection. n=8-17 animals per group. Dunn's test with Holm correction.
(P) Relative reduction in blood glucose compared to pre-infection levels from 24-hr experiment. n=8-17 animals per group. Dunn's test with Holm correction.

(Q) Serum GDF15 levels from the 24-hr experiment. n=7-17 animals per group. Dunn's test with Holm correction.
(A to Q) Pooled from two independent repeats.

Figure 1

See image above for figure legend.

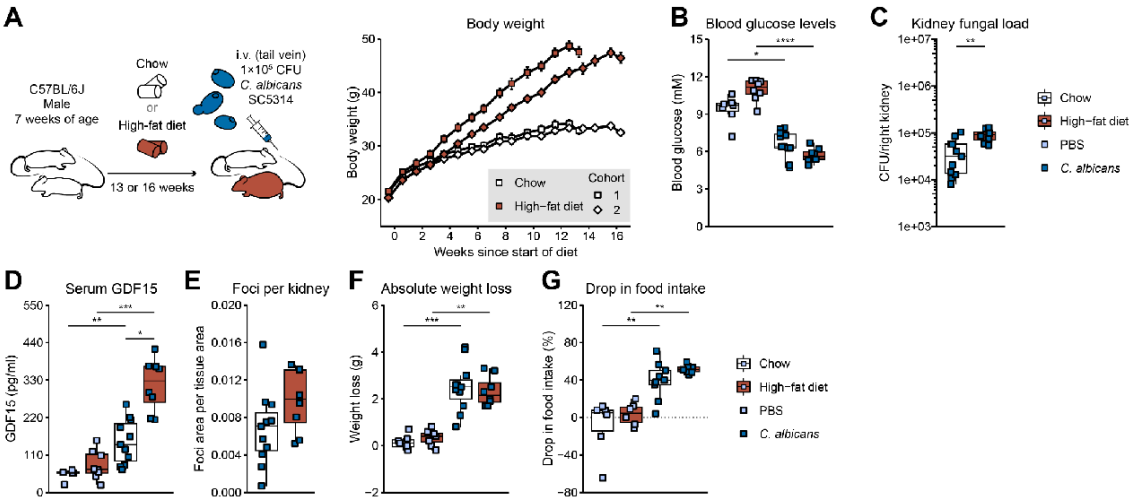


Figure 2. High-fat diet-induced obesity worsens *Candida* disease but only partially recapitulates the T2D phenotype

(A) 7-week-old male C57BL/6J mice were placed on a high-fat diet for 13 (cohort 1) or 16 (cohort 2) weeks prior to intravenous infection with 1×10^5 CFU *C. albicans*. Graph shows body weight over diet-feeding period.
(B) Blood glucose levels at 24 hours post-infection. n=7-11 animals per group. Dunn's test with Holm correction.
(C) Kidney fungal load of infected animals at 24 hours post-infection. n=8-11 animals per group. Mann-Whitney *U* test.
(D) Serum GDF15 levels by ELISA. n=7-11 animals per group. Dunn's test with Holm correction.
(E) Area of inflammatory foci in H&E-stained kidney sections from infected mice relative to total kidney area. n=8-11 animals per group. Mann-Whitney *U* test ($p > 0.05$).
(F) Absolute weight loss at 24 hours post-infection. n=7-11 animals per group. Dunn's test with Holm correction.
(G) Relative drop in food intake compared to pre-infection levels at 24 hours post-infection. n=6-9 animals per group. Dunn's test with Holm correction.
(A to G) Pooled from two independent infection repeats (both cohorts placed on experimental diet at the same time).

Figure 2

See image above for figure legend.

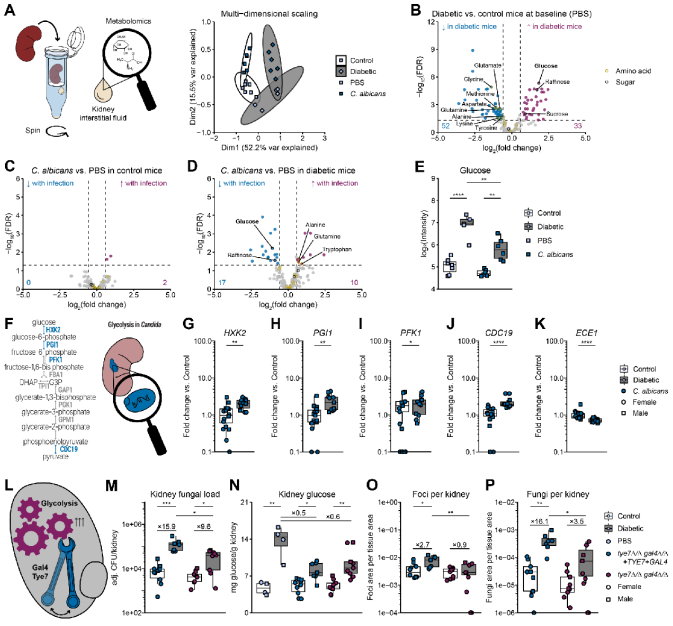


Figure 3. *C. albicans* exploits poor glycaemic control in T2D hosts to drive its own growth

(A) 8- to 12-week-old male T2D (db/db) and control mice were intravenously infected with 1×10^5 CFU *C. albicans*, and tissues were harvested at 24 hours post-infection. Kidney interstitial fluid was collected through centrifugation, and metabolite levels were measured using untargeted metabolomics. Plot shows multi-dimensional scaling based on correlation distances. n=5-7 animals per group.

(B to D) Volcano plot showing differences in metabolite abundance between uninfected T2D mice and controls (B), control mice with or without infection (C) and T2D mice with or without infection (D).

(E) Abundance of glucose from metabolomics data. n=5-7 animals per group. Shown are false-discovery rates from limma statistics.

(F) Schematic showing genes involved in glycolysis in *C. albicans*. In blue are genes assessed by qPCR in panels G-J.

(G to K) Expression of fungal glycolysis (G to J) or virulence (K) genes in infected kidneys of T2D and control mice (same cohort as Figure 1J-Q) relative to fungal housekeeping genes *18S* and *RDN25*, expressed as fold change from control. n=11-17 animals per group. Mann-Whitney *U* test.

(L) *C. albicans* transcription factors Tye7 and Gal4 cooperatively regulate glycolytic gene expression. 10- to 12-week-old T2D (db/db) and control mice of both sexes were intravenously infected with 1×10^5 CFU of the *tye7*Δ/Δ*gal4*Δ/Δ double mutant or a complemented control strain (*tye7*Δ/Δ*gal4*Δ/Δ+*TYE7*+*GAL4*). Mice were culled and tissues harvested at 24 hours post-infection.

(M) Kidney fungal load of infected mice, adjusted for infection inoculum. Median fold differences between indicated groups are shown. n=7-10 animals per group. Dunn's test with Holm correction.

(N) Kidney glucose levels. Median fold differences between indicated groups are shown. n=4-10 animals per group. Dunn's test with Holm correction.

(O) Area of inflammatory foci in PAS-stained kidney sections from infected mice relative to total kidney area. Median fold differences between indicated groups are shown. n=7-10 animals per group. Dunn's test with Holm correction.

(P) Area of PAS$^+$ fungi in PAS-stained kidney sections from infected mice relative to total kidney area. Median fold differences between indicated groups are shown. n=7-10 animals per group. Dunn's test with Holm correction. \

(A to E) Single experiment. (F-P) Pooled from two independent repeats.

Figure 3

See image above for figure legend.

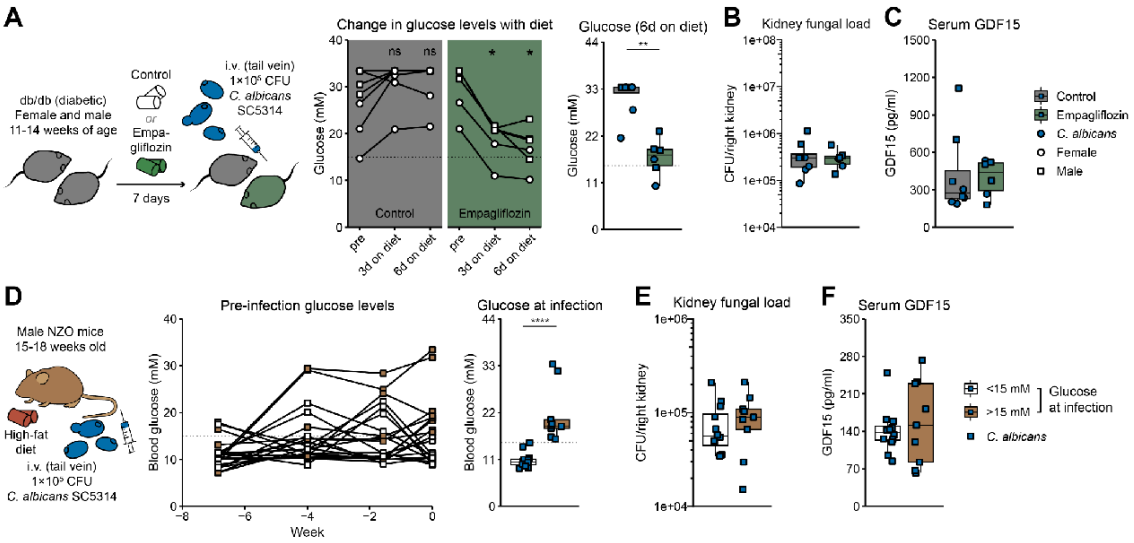


Figure 4. Chronic metabolic dysfunction, not glucose levels at infection, increases *Candida* disease susceptibility

(A) 11-14-week-old T2D (db/db) mice of both sexes were placed on a 0.03% empagliflozin or control diet. After 7 days of diet feeding, mice were intravenously infected with 1×10^5 CFU *C. albicans* and culled 24 hours post-infection. Graph shows blood glucose levels throughout the diet-feeding period. n=6-8 animals per group. Left, Wilcoxon signed-rank test between time points; right, Mann-Whitney *U* test between groups.

(B) Kidney fungal load at 24 hours post-infection. n=6-8 animals per group. Mann-Whitney *U* test ($p > 0.05$).

(C) Serum GDF15 levels by ELISA at 24 hours post-infection. n=6-8 animals per group. Mann-Whitney *U* test ($p > 0.05$).

(D) 15-18-week-old male NZO mice were placed on a high-fat diet until ~50% of mice had shown blood glucose levels >15 mM. Blood glucose levels were measured again immediately prior to intravenous infection with 1×10^5 CFU *C. albicans*, and mice were culled at 24 hours post-infection. Graph shows blood glucose levels in the lead-up to infection. n=21 animals.

(E) Kidney fungal load at 24 hours post-infection, stratified by blood glucose levels immediately prior to infection. n=9-11 animals per group. Mann-Whitney *U* test ($p > 0.05$).

(F) Serum GDF15 levels by ELISA at 24 hours post-infection. n=9-11 animals per group. Mann-Whitney *U* test ($p > 0.05$).

(A to F) Single experiment.

Figure 4

See image above for figure legend.

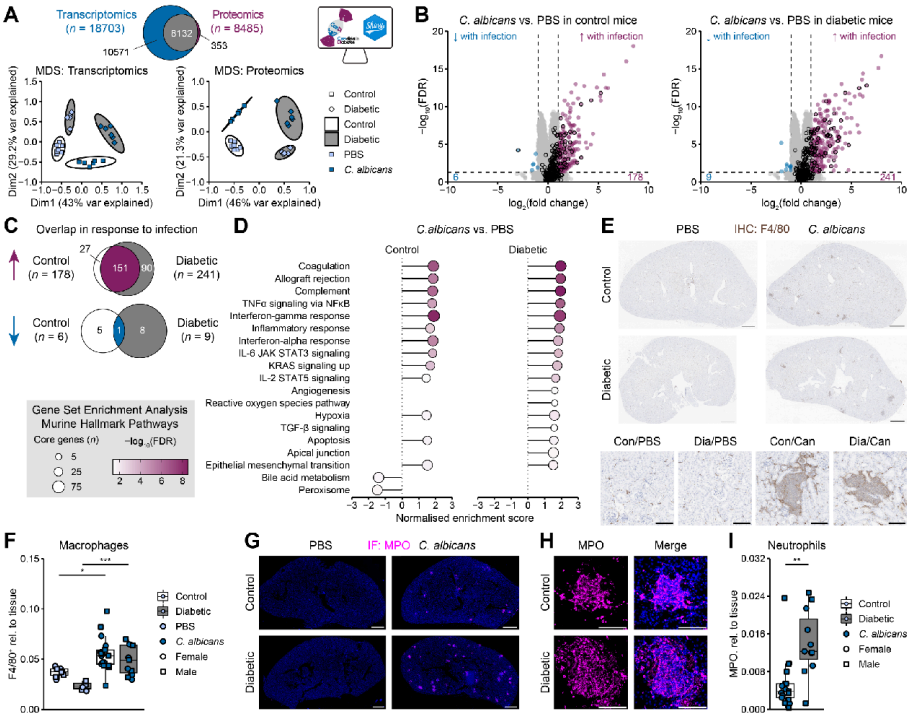


Figure 5. T2D mice mount antifungal immune responses comparable to controls.
(A) Kidney homogenates from male T2D (db/db) and control mice infected with *C. albicans* for 24 hours (same cohort as in Figure 3A-E) were analysed by bulk RNA sequencing (transcriptomics) and Liquid chromatography–mass spectrometry (proteomics). Plots show overlap in detected analytes between methods and multi-dimensional scaling based on correlation distances for each data set. n=5-7 animals per group. Data can be explored using the interactive CanDi (Candida in Diabetes) app (https://github.com/hstoelting/CanDi).
(B) Volcano plots showing changes in protein expression with infection in control (left) or T2D (right) mice. Proteins involved in immune-related Hallmark pathways (*Complement*, *IL2 STAT5 Signalling*, *IL6 JAK STAT3 Signalling*, *Inflammatory Response*, *Interferon Alpha Response*, *Interferon Gamma Response*, *Reactive Oxygen Species Pathway*, *TNFα Signalling via NFκB*) are highlighted by black outlines. n=5-7 animals per group.
(C) Overlap in proteins up- (top) or downregulated (bottom) with infection in control and T2D mice.
(D) Gene set enrichment analysis of changes in protein expression with infection in control (left) and T2D (right) mice, based on murine Hallmark pathways. Only significantly enriched pathways are shown.
(E) Immunohistochemical staining for F4/80 in kidney sections from T2D and control mice infected with *C. albicans* for 24 hours (same cohort as in Figure 1J-Q). Size of scale bar: 1 mm, overview; 100 µm, zoom.
(F) Quantification of (E). F4/80$^+$ area relative to total kidney area. n=7-17 animals per group. Dunn's test with Holm correction.
(G) Immunofluorescence staining for myeloperoxidase (MPO; magenta) in kidney sections from T2D and control mice infected with *C. albicans* for 24 hours (same cohort as in Figure 1J-Q). Nuclei stained with DAPI (blue). Size of scale bar: 1 mm, overview.
(H) Zoomed-in images of MPO staining of kidneys from infected T2D and control mice. Colours: blue, DAPI; magenta, MPO. Size of scale bar: 100 µm.
(I) Quantification of (H). MPO$^+$ area relative to total kidney area. n=11-17 animals per group. Mann-Whitney *U* test.
(A to D) Single experiment. (E to I) Pooled from two independent repeats.

Figure 5

See image above for figure legend.

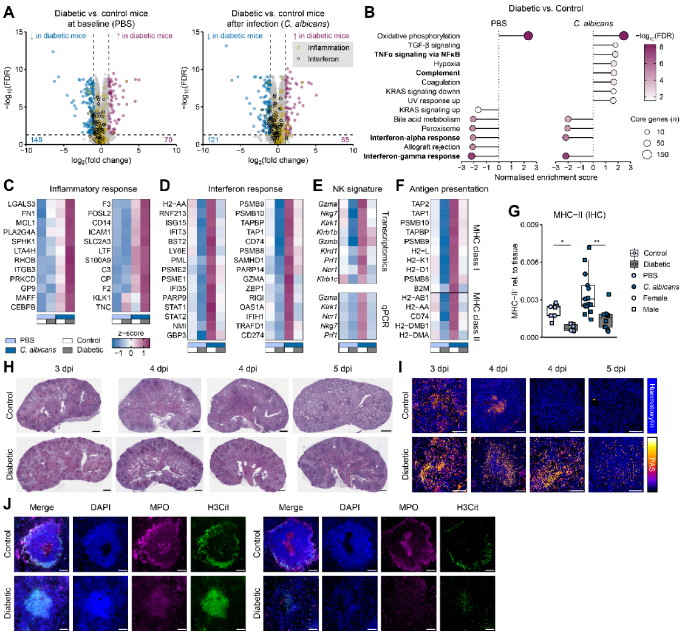


Figure 6. T2D mice display stunted interferon and NK cell signatures and fail to restrict *C. albicans* infection

(A) Volcano plots showing differences in protein expression between uninfected (left) or infected (right) T2D and control animals. Proteins involved in Hallmark pathways related to inflammation (*Complement*, *Inflammatory Response*, *TNFα signalling via NFκB*) or interferon (*Interferon Alpha Response*, *Interferon Gamma Response*) are highlighted by yellow or black outlines, respectively.

(B) Gene set enrichment analysis of differences in protein expression between uninfected (left) or infected (right) T2D and control mice, based on murine Hallmark pathways. Only significantly enriched pathways are shown.

(C and D) Heatmaps showing scaled expression levels of proteins involved in inflammatory (C) or interferon (D) response. All depicted proteins were significantly upregulated in control kidneys with infection (C and D) and expressed at significantly higher (C) or lower (D) levels in infected T2D animals (FDR < 0.05). n=5-7 animals per group.

(E) Heatmaps showing scaled expression levels of NK cell-related genes from kidney transcriptomics (top; same cohort as in Figure 3A-E; n=5-7 animals per group) or qPCR (bottom; same cohort as in Figure 1J-Q; n=8-17 animals per group).

(F) Heatmap showing scaled expression levels of proteins involved in antigen presentation. n=5-7 animals per group.

(G) MHC-II$^+$ area relative to total kidney area from immunohistochemical staining. n=6-17 animals per group. Dunn's test with Holm correction.

(H) Representative images of PAS staining of kidney sections from T2D and control mice infected with *C. albicans* at humane endpoint (same cohort as in Figure 1A-I). Size of scale bar: 1 mm.

(I) Zoomed-in images of deconvoluted and pseudo-coloured PAS staining of kidneys from T2D and control mice collected at humane endpoint. Colours: blue, haematoxylin; fire scale, PAS. Size of scale bar: 100 µm.

(J) Representative images of immunofluorescence staining for MPO (magenta) and citrullinated histone H3 (H3Cit; green) in kidneys of T2D and control mice that reached their humane endpoint at 4 days post-infection. Nuclei counterstained with DAPI (blue). Size of scale bar: 100 µm.

(A to F) Single experiment (except E qPCR panel). (G to J and E qPCR panel) Pooled from two independent repeats.

Figure 6

See image above for figure legend.

Supplementary Files

This is a list of supplementary files associated with this preprint. Click to download.

- StoeltingetalDocumentS1small.pdf